

Theoretical concepts and measurement prospects for BSM trilinear couplings: a case study for scalar top quarks

Henning Bahl^{*1}, Johannes Braathen^{†2}, and Georg Weiglein^{‡2,3}

¹*University of Chicago, Department of Physics, 5720 South Ellis Avenue, Chicago, IL 60637 USA*

²*Deutsches Elektronen-Synchrotron DESY, Notkestr. 85, 22607 Hamburg, Germany*

³*II. Institut für Theoretische Physik, Universität Hamburg, Luruper Chaussee 149, 22761 Hamburg, Germany*

After the possible discovery of new heavy particles at the LHC, it will be crucial to determine the properties and the underlying physics of the new states. In this work, we focus on scalar trilinear couplings, employing as an example the case of the trilinear coupling of scalar partners of the top quark to the Higgs boson. We discuss possible strategies for experimentally determining the scalar top (stop) trilinear coupling parameter, which controls the stop–stop–Higgs interaction, and we demonstrate the impact of different renormalisation prescriptions for this parameter. We find that the best prospects for determining the stop trilinear coupling arise from its quantum effects entering the model prediction for the mass of the SM-like Higgs boson in comparison to the measured value. We point out that the prediction for the Higgs-boson mass has a high sensitivity to the stop trilinear coupling even for heavy masses of the non-standard particles. Regarding the renormalisation of the stop trilinear coupling we identify a renormalisation scheme that is preferred in view of the present level of accuracy and we clarify the source of potentially large logarithms that cannot be resummed with standard renormalisation group methods.

^{*}hbahl@uchicago.edu

[†]johannes.braathen@desy.de

[‡]georg.weiglein@desy.de

Contents

| | |
|---|-----------|
| 1. Introduction | 3 |
| 2. The stop mixing parameter | 4 |
| 3. Measurement of the stop mixing parameter | 5 |
| 3.1. Stop masses | 6 |
| 3.2. Stop mixing angle | 7 |
| 3.3. Higgs–stop–stop interaction | 9 |
| 3.4. Relation to the mass and the couplings of the SM-like Higgs boson | 11 |
| 4. Renormalisation of the stop sector | 14 |
| 4.1. $\overline{\text{DR}}$ scheme | 16 |
| 4.2. Process-dependent OS scheme | 16 |
| 4.3. Process-independent OS scheme | 16 |
| 4.4. $\overline{\text{MDR}}$ and $\overline{\text{DR}}$ scheme | 17 |
| 4.5. Mixed schemes | 17 |
| 5. Renormalisation of the stop mixing parameter and the prediction for the mass of the SM-like Higgs boson | 18 |
| 6. Conclusions | 23 |
| A. Bottom-Yukawa corrections to the X_t conversion | 26 |

1. Introduction

So far, only one scalar particle without a known substructure has been found: the Higgs boson with a mass of about 125 GeV discovered at the Large Hadron Collider (LHC) in 2012 [1, 2]. Within the Standard Model (SM) of particle physics, the detected Higgs boson is identified with the Higgs boson that is predicted as the only fundamental scalar in this model. However, in many extensions of the SM by physics beyond the SM (BSM) additional scalar degrees of freedom are introduced in order to address questions that are unresolved in the SM, for instance the nature of dark matter, the origin of neutrino masses, or the observed baryon asymmetry of the universe.

Additional spin-zero particles can either be introduced by extending the SM Higgs sector, for example singlet extensions of the SM, two-Higgs-doublet models, etc., or by adding a completely new scalar sector, for example in supersymmetric (SUSY) theories, which associate a scalar degree of freedom with each fermion degree of freedom. A particular new type of interaction potentially arising in these models is an interaction between three scalars that is not generated by a vacuum expectation value. This type of interaction is forbidden in the SM due to the $SU(2)_L$ gauge symmetry of the model. Correspondingly, the trilinear interaction of the SM Higgs boson is generated only after electroweak symmetry breaking. In BSM theories, trilinear scalar couplings can, however, arise as a consequence of dimensionful couplings independently of spontaneous symmetry breaking.

These dimensionful couplings appear for instance in extensions of the SM Higgs sector by one or more scalar gauge singlet(s) if no \mathbb{Z}_2 symmetry is imposed [3–5]. Another example are supersymmetric theories which predict trilinear couplings between the Higgs bosons and the supersymmetric partners of the SM fermions. Among these couplings, the trilinear coupling between the supersymmetric partners of the top quark (which are usually called scalar top quarks or stops) and the SM-like Higgs boson is of particular importance. This “stop mixing parameter” is typically the largest among the trilinear couplings and controls not only the Higgs–stop–stop interaction itself but also the mass splitting between the stops.

If an extended scalar sector is discovered at the LHC or a future collider, the measurement of the interactions between the various scalars will be crucial to pinpoint the underlying theory. With this motivation in mind, we discuss in this paper how trilinear scalar couplings should be properly defined in the theoretical predictions and how they can be extracted from experimental measurements. We focus our discussion on the example of the stop mixing parameter of the Minimal Supersymmetric SM (MSSM), building upon earlier work in the literature [6–14]. We will also point out aspects of our discussion that are valid for other theories with trilinear scalar couplings.

We review different ways to extract the stop mixing parameters from experimental measurements. Going beyond existing results, we point out the difficulties of the various approaches and emphasise the crucial role of the mass of the SM-like Higgs boson. In connection with this discussion, we compare different known schemes [15–31] for the renormalisation of the stop mixing parameter in Higgs boson mass calculations, and we examine what scheme choice would be most appropriate. In this context, we ascertain

the origin of large Sudakov-like logarithms plaguing the Higgs boson mass calculation in the on-shell scheme when combining diagrammatic and EFT techniques. Based on this discussion, we propose to use a mixed scheme where the stop mixing parameter is renormalised in the $\overline{\text{DR}}/\overline{\text{MDR}}$ scheme while the stop masses are renormalised on-shell.

This work is structured as follows. We present a short review of the MSSM stop sector in Section 2. In Section 3, we point out difficulties in measuring the stop mixing parameter in various approaches. Based on this discussion, we review different possibilities to renormalise the stop sector in Section 4. In Section 5, we discuss the origin of Sudakov-like logarithms affecting Higgs mass calculations in the on-shell scheme incorporating renormalisation-group resummations. Our conclusions can be found in Section 6. Appendix A provides additional details regarding the conversion of the stop mixing parameter between the on-shell and the $\overline{\text{DR}}$ scheme.

2. The stop mixing parameter

In the MSSM, trilinear scalar couplings can arise from terms in the superpotential — in the form of the μ parameter — as well as from the soft SUSY-breaking Lagrangian — in the form of the trilinear couplings A_f . We focus here on the interaction of stops with Higgs bosons.

As a first consequence of the Higgs–stop–stop interaction, mixing between the superpartners of the left- and right-handed components of the top quark, which we denote by \tilde{t}_L and \tilde{t}_R , respectively, is induced. This is directly visible in the stop mass matrix which takes the following form,

$$\mathbf{M}_{\tilde{t}} = \begin{pmatrix} m_{\tilde{t}_L}^2 + m_t^2 + \cos(2\beta)(\frac{1}{2} - \frac{2}{3}s_W^2)M_Z^2 & m_t X_t^* \\ m_t X_t & m_{\tilde{t}_R}^2 + m_t^2 + \frac{2}{3}\cos(2\beta)s_W^2 M_Z^2 \end{pmatrix}, \quad (1)$$

where $m_{\tilde{t}_{L,R}}^2$ are the stop soft SUSY-breaking masses, and $X_t \equiv A_t - \mu^*/\tan\beta$ is the stop mixing parameter ($\tan\beta$ denotes the ratio of the Higgs vacuum expectation values, $\tan\beta \equiv t_\beta \equiv v_u/v_d$). M_Z is the mass of the Z boson and s_W the sine of the weak mixing angle. m_t is the top-quark mass, for which we will use a value of 173.2 GeV throughout this paper.

The stop mass matrix can be diagonalised by a unitary transformation,

$$\begin{pmatrix} \tilde{t}_1 \\ \tilde{t}_2 \end{pmatrix} = \mathbf{U}_{\tilde{t}} \begin{pmatrix} \tilde{t}_L \\ \tilde{t}_R \end{pmatrix} \quad (2)$$

such that

$$\mathbf{U}_{\tilde{t}} \mathbf{M}_{\tilde{t}} \mathbf{U}_{\tilde{t}}^\dagger = \text{diag}(m_{\tilde{t}_1}^2, m_{\tilde{t}_2}^2), \quad \text{with} \quad \mathbf{U}_{\tilde{t}} = \begin{pmatrix} c_{\tilde{t}} & s_{\tilde{t}} e^{-i\phi_{X_t}} \\ -s_{\tilde{t}} e^{i\phi_{X_t}} & c_{\tilde{t}} \end{pmatrix}, \quad \mathbf{U}_{\tilde{t}} \mathbf{U}_{\tilde{t}}^\dagger = \mathbb{1}. \quad (3)$$

Here $m_{\tilde{t}_1}^2 \leq m_{\tilde{t}_2}^2$ by definition,

$$\phi_{X_t} = \arg(X_t), \quad (4)$$

and we introduced the abbreviations $s_\gamma \equiv \sin \gamma$ and $c_\gamma \equiv \cos \gamma$ for a generic angle γ .

The mixing angle $\theta_{\tilde{t}}$ obeys the relation

$$\cos(2\theta_{\tilde{t}}) = \frac{m_{\tilde{t}_R}^2 - m_{\tilde{t}_L}^2 - M_Z^2 c_{2\beta} \left(\frac{1}{2} - \frac{4}{3}s_W^2\right)}{m_{\tilde{t}_2}^2 - m_{\tilde{t}_1}^2}, \quad (5)$$

where the stop masses are given by

$$m_{\tilde{t}_{1,2}}^2 = m_t^2 + \frac{1}{2} \left\{ m_{\tilde{t}_L}^2 + m_{\tilde{t}_R}^2 \mp \sqrt{\left[m_{\tilde{t}_L}^2 - m_{\tilde{t}_R}^2 + M_Z^2 c_{2\beta} \left(\frac{1}{2} - \frac{4}{3}s_W^2\right) \right]^2 + 4m_t^2 |X_t|^2} \right\}. \quad (6)$$

For later use, we define the abbreviations

$$M_{\text{SUSY}} = \sqrt{m_{\tilde{t}_L} m_{\tilde{t}_R}}, \quad \hat{X}_t = X_t / M_{\text{SUSY}}. \quad (7)$$

The Higgs–stop–stop interaction is, however, not only manifest in the stop mass matrix but also induces a direct coupling of the light \mathcal{CP} -even Higgs boson h to two stops. In the limit of vanishing electroweak gauge couplings, these couplings read

$$c(h\tilde{t}_1\tilde{t}_1) = -2i \frac{m_t}{v} (m_t + s_{\theta_{\tilde{t}}} c_{\theta_{\tilde{t}}} |X_t|), \quad (8)$$

$$c(h\tilde{t}_1\tilde{t}_2) = -i \frac{m_t}{v} c_{2\theta_{\tilde{t}}} |X_t| e^{i\phi_{X_t}}, \quad (9)$$

$$c(h\tilde{t}_2\tilde{t}_2) = -2i \frac{m_t}{v} (m_t - s_{\theta_{\tilde{t}}} c_{\theta_{\tilde{t}}} |X_t|), \quad (10)$$

where $v \simeq 246$ GeV denotes the vacuum expectation value (vev), with $v^2 = v_u^2 + v_d^2$.

3. Measurement of the stop mixing parameter

As discussed in Section 2, the stop mixing parameter X_t induces mixing between the left- and right-handed stops. Therefore, observables depending on the stop mixing are also sensitive to the stop mixing parameter. Since the stop mixing parameter X_t also appears directly in the Higgs–stop–stop interaction, measuring processes involving a Higgs boson and two stops as external particles allows one to directly constrain X_t without resorting to its relation to the stop mixing angle. Moreover, the Higgs–stop–stop interaction can additionally influence other observables at the quantum level, such as the predictions for the Higgs boson masses. We note that the observations in this section (with the exception of the Higgs mass predictions) also apply to other BSM theories with trilinear couplings between three different particles.

In the following, we will discuss these different possibilities in detail and qualitatively assess their prospects for experimentally determining the parameter X_t at the LHC and future high-energy colliders. We will in the following mainly restrict ourselves to the case where the parameter X_t is real. Prospects for measuring the phase of X_t are discussed in Ref. [10].

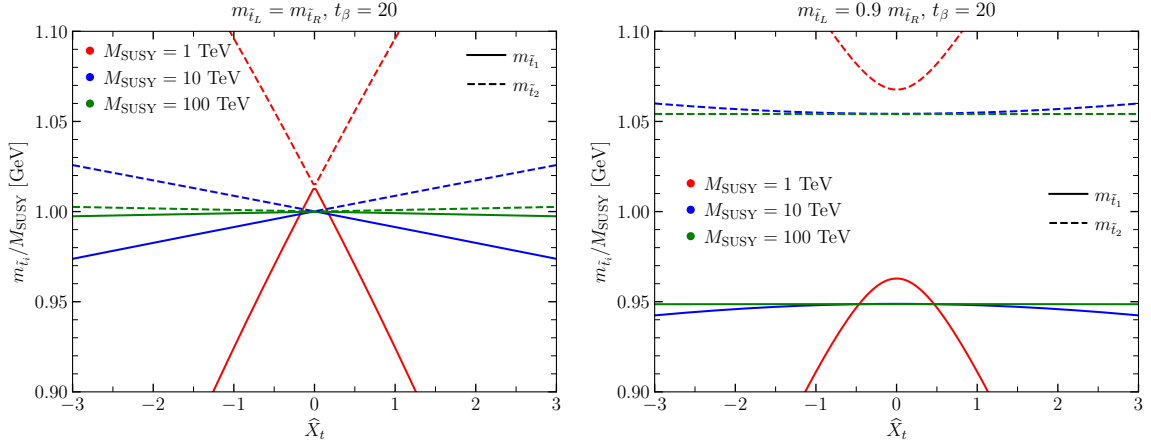


Figure 1: Dependence of the (tree-level) stop masses on \hat{X}_t for $m_{\tilde{t}_L} = m_{\tilde{t}_R}$ (left) and $m_{\tilde{t}_L} = 0.9 m_{\tilde{t}_R}$ (right) for $\tan \beta = 20$. Results for the light (solid curves) and heavy (dashed curves) stop mass eigenstates, normalised to M_{SUSY} , are shown for different values of M_{SUSY} , namely: $M_{\text{SUSY}} = 1$ TeV (red), $M_{\text{SUSY}} = 10$ TeV (blue) and $M_{\text{SUSY}} = 100$ TeV (green).

3.1. Stop masses

In general three experimental inputs are needed in order to constrain the three parameters X_t , $m_{\tilde{t}_L}$ and $m_{\tilde{t}_R}$, which affect the stop masses and the stop mixing angle as detailed in Section 2. Thus, a determination of X_t just from the measured values of the two stop masses is only possible if a certain relation between $m_{\tilde{t}_L}$ and $m_{\tilde{t}_R}$ is assumed. The dependence of the stop masses on X_t is illustrated in Fig. 1 for the two cases $m_{\tilde{t}_L} = m_{\tilde{t}_R} = M_{\text{SUSY}}$ (left) and $m_{\tilde{t}_L} = 0.9 m_{\tilde{t}_R}$ (right). In both plots the lighter stop mass (solid curves) and the heavier stop mass (dashed curves), normalised by their geometric mean M_{SUSY} , are shown for $M_{\text{SUSY}} = 1$ TeV (red), $M_{\text{SUSY}} = 10$ TeV (blue), and $M_{\text{SUSY}} = 100$ TeV (green), and $\tan \beta = 20$ has been chosen.

In the left plot the dependence of the stop masses on \hat{X}_t is quite pronounced for $M_{\text{SUSY}} = 1$ TeV, while the slope of the curves gets significantly smaller with larger M_{SUSY} . Especially for $M_{\text{SUSY}} = 100$ TeV a very high mass resolution would be required to extract X_t from the measured stop mass values. As is illustrated in the right plot of Fig. 1, changing the assumption on the soft SUSY-breaking parameters from $m_{\tilde{t}_L} = m_{\tilde{t}_R}$ to $m_{\tilde{t}_L} = 0.9 m_{\tilde{t}_R}$ has a large impact. In this case, the mass difference between the two stops is rather large, while the dependence on X_t is diminished. The prospects for determining X_t from the stop masses would be significantly worse than for the case with $m_{\tilde{t}_L} = m_{\tilde{t}_R}$, in particular for M_{SUSY} values in excess of 10 TeV.

These simple examples underline the obvious fact that in general it is not possible to disentangle to what extent the mass difference between the two stop masses is caused by stop mixing or by a splitting between the stop soft SUSY-breaking parameters. Accordingly, measurements of just the two stop masses alone will of course not be sufficient to determine X_t .

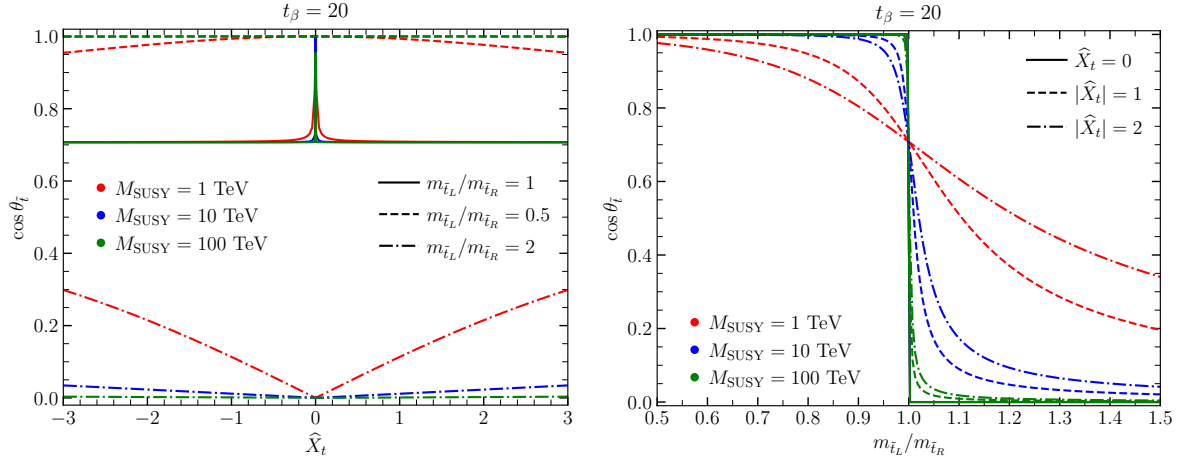


Figure 2: Cosine of the stop mixing angle as a function of \hat{X}_t (*left*) and as a function of $m_{\tilde{t}_L}/m_{\tilde{t}_R}$ (*right*) for different values of M_{SUSY} and $\tan\beta = 20$.

3.2. Stop mixing angle

As discussed in Section 2, the stop mixing angle determines the mixing between the stop gauge eigenstates \tilde{t}_L and \tilde{t}_R . Consequently, processes involving stops that are induced by the $SU(2)_L$ interaction are sensitive to the stop mixing angle.

At hadron colliders like the LHC, stops are predominantly produced via QCD interactions. Therefore, the branching ratios of the stops need to be disentangled and measured precisely in order to extract the stop mixing angle, which is experimentally challenging (see Ref. [10] for an exploratory study).¹

At lepton colliders, the stop mixing angle could be extracted more easily, since the stops can potentially be produced with a sizeable rate via processes involving the electroweak gauge bosons [6–9]. However, stops with masses of a few TeV may be beyond the kinematic reach of the next generation of e^+e^- colliders.

Even if a measurement of the stop mixing angle becomes possible, it is important to take into account that the fundamental parameter of the underlying theory is not the stop mixing angle but in fact the stop mixing parameter X_t . From the measured values of the two stop masses and the stop mixing angle it is in principle possible to determine the model parameters X_t , $m_{\tilde{t}_L}$ and $m_{\tilde{t}_R}$. However, as is illustrated in Fig. 2, even a precise measurement of the stop mixing angle (together with measurements of the stop masses) does not necessarily allow a reliable determination of the stop mixing parameter.

The left panel of Fig. 2 shows the cosine of the stop mixing angle derived at the tree level as a function of \hat{X}_t (all interactions induced by $SU(2)_L$ interactions are proportional to $\cos\theta_{\tilde{t}}$). Results are shown for three different values of M_{SUSY} — 1 TeV (red), 10 TeV (blue), 100 TeV (green) — and three different values of $m_{\tilde{t}_L}/m_{\tilde{t}_R}$ — 1 (solid lines), 0.5

¹Another possibility would be to measure the kinematic shapes of decay processes like $\tilde{t}_{1,2} \rightarrow t\tilde{\chi}$, where $\tilde{\chi}$ is a neutralino. This is, however, experimentally even more challenging.

(dashed lines), 2 (dot-dashed lines). One can see that the determination of X_t from a given input for $\cos\theta_{\tilde{t}}$ (and for $m_{\tilde{t}_1}, m_{\tilde{t}_2}$) will only be possible with a good sensitivity if the overall stop mass scale is not too large and if there is a significant splitting between the stop soft SUSY-breaking parameters. For $m_{\tilde{t}_L} = m_{\tilde{t}_R}$, the two diagonal entries of the stop mass matrix are approximately equal to each other (up to electroweak terms). In this situation, the size of the off-diagonal entries, controlled by X_t , has only a minor impact on the mixing angle, whose cosine is $\sim 1/\sqrt{2}$. An exception are only X_t values very close to zero, where the cosine of the stop mixing angle as a function of X_t develops a sharp peak towards $\cos\theta_{\tilde{t}} = 1$, which is reached for $X_t = 0$. This behaviour is a consequence of the electroweak contributions and the condition that $m_{\tilde{t}_1} \leq m_{\tilde{t}_2}$. For increasing M_{SUSY} , the numerical impact of the electroweak terms becomes smaller and smaller, resulting in a sharper peak. In the case of a sizeable splitting between $m_{\tilde{t}_L}$ and $m_{\tilde{t}_R}$, displayed in our example for $m_{\tilde{t}_L}/m_{\tilde{t}_R} = 0.5$ and 2, the stop mixing angle depends more sensitively on X_t if M_{SUSY} is around the TeV scale. For larger M_{SUSY} the dependence becomes more and more flat. This is a consequence of the fact that the diagonal entries of the stop mass matrix are of $\mathcal{O}(M_{\text{SUSY}}^2)$ while the off-diagonal entries are of $\mathcal{O}(m_t M_{\text{SUSY}})$.

The dependence on $m_{\tilde{t}_L}/m_{\tilde{t}_R}$ is further explored in the right panel of Fig. 2 showing the cosine of the stop mixing angle, once again computed at tree level, as a function of $m_{\tilde{t}_L}/m_{\tilde{t}_R}$. The results are shown for three different values of M_{SUSY} — 1 TeV (red), 10 TeV (blue), 100 TeV (green) — and three different values of $|\hat{X}_t|$ — 0 (solid lines), 1 (dashed lines), 2 (dot-dashed lines),² while $\tan\beta$ is set to 20.

For $\hat{X}_t = 0$, the stops do not mix, and the stop mixing angle does not depend on M_{SUSY} . Consequently, all solid lines lie on top of each other. The step at $m_{\tilde{t}_L}/m_{\tilde{t}_R} = 1$ is a consequence of demanding $m_{\tilde{t}_1} \leq m_{\tilde{t}_2}$. While for $M_{\text{SUSY}} = 1$ TeV the different $|\hat{X}_t|$ curves are still well separated for $m_{\tilde{t}_L}/m_{\tilde{t}_R} \lesssim 0.8$ and $m_{\tilde{t}_L}/m_{\tilde{t}_R} \gtrsim 1.1$, the curves approach each other for rising M_{SUSY} implying the need for more and more precise measurements of $m_{\tilde{t}_L}$, $m_{\tilde{t}_R}$ and $\cos\theta_{\tilde{t}}$ in order to extract X_t .

In summary, a precise extraction of the stop mixing parameter from the measurement of the stop mixing angle (in combination with the measurements of the two stop masses) is only possible if there is a large splitting between the soft SUSY-breaking parameters in the stop sector and if the overall stop mass scale (i.e. the mean of the stop masses) is close to the TeV scale. If, on the other hand, the experimental information on the two stop masses and the stop mixing angle reveals that an approximate equality $m_{\tilde{t}_L} \approx m_{\tilde{t}_R}$ holds, the dependence of the stop masses on X_t as discussed in Fig. 1 can be utilised to constrain X_t . However, also in this case the sensitivity to X_t is significantly diminished for stop masses in the multi-TeV regime (see the discussion above). While at first sight it might seem that at a collider of sufficient energy that has the capability for precise measurements of the stop masses and the stop mixing angle it should be possible to obtain a precise determination of the stop mixing parameter also for stop masses beyond

²The cosine of the mixing angle does not depend on the sign of \hat{X}_t as expected by the fact that the sign can be rewritten as a phase (see for instance Ref. [32]). This is also visible in the left panel of Fig. 2.

the TeV scale, this is in fact not the case as a consequence of contributions that scale like m_t/M_{SUSY} .

3.3. Higgs–stop–stop interaction

Another possibility for experimentally probing X_t is the investigation of observables involving the Higgs–stop–stop interaction at the tree level. In this context, the decay $\tilde{t}_2 \rightarrow \tilde{t}_1 + h$ appears to be most promising.³

The associated \tilde{t}_2 decay width is given by

$$d\Gamma_{\tilde{t}_2 \rightarrow \tilde{t}_1 h} = \frac{1}{64\pi^2} \frac{\sqrt{(m_{\tilde{t}_2}^2 - (m_{\tilde{t}_1} + m_h)^2)(m_{\tilde{t}_2}^2 - (m_{\tilde{t}_1} - m_h)^2)}}{m_{\tilde{t}_2}^3} |\mathcal{M}(\tilde{t}_2 \rightarrow \tilde{t}_1 h)|^2 d\cos\theta, \quad (11)$$

where θ is the angle between the 3-momenta of the final state particles. The matrix element $\mathcal{M}(\tilde{t}_2 \rightarrow \tilde{t}_1 h)$ is proportional to X_t (see Eq. (9)).

It is instructive to discuss the limiting kinematic cases for this decay. First, we consider the case in which the heavier stop is much heavier than the SM-like Higgs boson and the lighter stop ($m_{\tilde{t}_1}, m_h \ll m_{\tilde{t}_2}$). In this case, the total decay width behaves as

$$d\Gamma_{\tilde{t}_2 \rightarrow \tilde{t}_1 h} \xrightarrow{m_h, m_{\tilde{t}_1} \ll m_{\tilde{t}_2}} \frac{1}{64\pi^2} \frac{1}{m_{\tilde{t}_2}} |\mathcal{M}(\tilde{t}_2 \rightarrow \tilde{t}_1 h)|^2 d\cos\theta \propto \frac{|X_t|^2}{m_{\tilde{t}_2}}, \quad (12)$$

where in the final step we only consider mass scales to obtain an estimate of the behaviour of the decay width. Assuming that $|X_t| \sim \mathcal{O}(M_{\text{SUSY}})$, then also $\Gamma_{\tilde{t}_2 \rightarrow \tilde{t}_1 h}$ is of $\mathcal{O}(M_{\text{SUSY}})$.

As a second limiting case, we consider the situation in which the two stops are approximately mass-degenerate and much heavier than the SM-like Higgs boson ($m_h \ll m_{\tilde{t}_1} \sim m_{\tilde{t}_2}$). In this limit the total decay width becomes

$$\begin{aligned} d\Gamma_{\tilde{t}_2 \rightarrow \tilde{t}_1 h} &\xrightarrow{m_h \ll m_{\tilde{t}_1} \sim m_{\tilde{t}_2}} \frac{1}{64\pi^2} \frac{|m_{\tilde{t}_2}^2 - m_{\tilde{t}_1}^2|}{m_{\tilde{t}_2}^3} |\mathcal{M}(\tilde{t}_2 \rightarrow \tilde{t}_1 h)|^2 d\cos\theta \simeq \\ &\simeq \frac{1}{64\pi^2} \frac{2m_t |X_t|}{m_{\tilde{t}_2}^3} |\mathcal{M}(\tilde{t}_2 \rightarrow \tilde{t}_1 h)|^2 d\cos\theta \propto \frac{m_t |X_t|^3}{m_{\tilde{t}_2}^3}. \end{aligned} \quad (13)$$

Comparing to Eq. (12), the decay width is suppressed by a factor of $m_t |X_t|/m_{\tilde{t}_2}^2$ in comparison to the case with $m_{\tilde{t}_1}, m_h \ll m_{\tilde{t}_2}$.⁴ Assuming again that $|X_t| \sim \mathcal{O}(M_{\text{SUSY}})$, $\Gamma_{\tilde{t}_2 \rightarrow \tilde{t}_1 h}$ is of $\mathcal{O}(m_t)$. This means that the decay width is much smaller than in the case of $m_h \sim m_{\tilde{t}_1} \ll m_{\tilde{t}_2}$, which is mainly due to the suppression of the phase space. Consequently, other decay channels of \tilde{t}_2 can easily dominate over the $\tilde{t}_2 \rightarrow \tilde{t}_1 + h$ decay channel in this case.

³Other processes like Higgs-induced di-stop production are experimentally much harder to access.

⁴As a consequence of expanding around $m_h/m_{\tilde{t}_{1,2}}$, we implicitly assumed the h boson to be massless, so that m_h does not appear in Eq. (13).

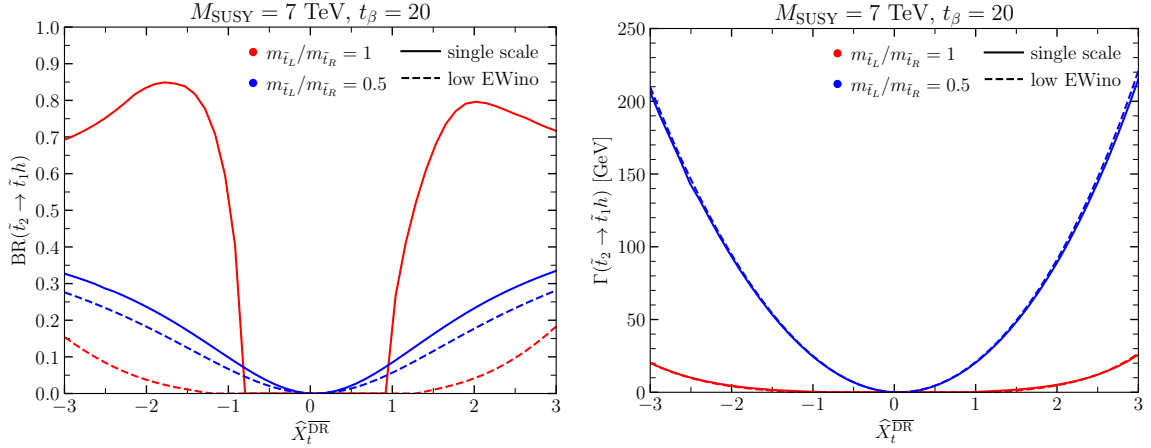


Figure 3: *Left*: branching ratio of \tilde{t}_2 into \tilde{t}_1 and a SM-like Higgs boson as a function of $\hat{X}_t^{\overline{\text{DR}}}$ for $m_{\tilde{t}_L}/m_{\tilde{t}_R} = 1$ (red lines) and $m_{\tilde{t}_L}/m_{\tilde{t}_R} = 0.5$ (blue lines). Results are shown for a single-scale scenario (solid lines) and a scenario with light EWinos (dashed lines). *Right*: same as left panel, but the $\tilde{t}_2 \rightarrow \tilde{t}_1 + h$ partial decay width is shown. The dashed lines lie on top of the solid lines.

We numerically investigate this behaviour in Fig. 3 showing the branching ratio of $\tilde{t}_2 \rightarrow \tilde{t}_1 + h$ (left panel) and the $\tilde{t}_2 \rightarrow \tilde{t}_1 + h$ partial decay width (right panel) as a function of \hat{X}_t , which for this Figure is chosen to be renormalised in the $\overline{\text{DR}}$ scheme, see below. The branching ratio and decay width are evaluated using SUSY-HIT [33–36], which includes the leading QCD corrections to $\tilde{t}_2 \rightarrow \tilde{t}_1 + h$, for two different scenarios: in the single scale scenario (solid curves), all soft SUSY-breaking masses (except for the stop SUSY-breaking masses) as well as the μ parameter and the mass scale of the heavy Higgs bosons are chosen to be equal to $M_{\text{SUSY}} = 7 \text{ TeV}$ (and $t_\beta = 20$ is used); for the low mass electroweakino scenario (dashed curves), the same parameters as in the single-scale scenario are used apart from the Wino and Bino soft SUSY-breaking masses (M_1 and M_2) as well as μ which are chosen to be equal to $M_{\text{SUSY}}/2$ (implying the existence of comparably lighter neutralinos and charginos). For the red curves, the stop soft-breaking masses are chosen to be equal to M_{SUSY} , while for the blue curves they are set to $m_{\tilde{t}_L} = M_{\text{SUSY}}/\sqrt{2}$ and $m_{\tilde{t}_R} = \sqrt{2}M_{\text{SUSY}}$.

We observe the largest branching ratio of $\sim 70 - 85\%$ in the single scale scenario with mass-degenerate stop soft-breaking masses for $|\hat{X}_t| > 1.5$ (see the left panel of Fig. 3). In this case, the $\tilde{t}_2 \rightarrow \tilde{t}_1 + h$ decay channel is enhanced by a factor $|\hat{X}_t|^3$ in comparison to the $\tilde{t}_2 \rightarrow \tilde{t}_1 + Z$ decay channel, the only other decay channel with a sizeable branching ratio. The $\tilde{t}_2 \rightarrow \tilde{t}_1 + h$ branching ratio, however, quickly goes to zero if $|\hat{X}_t|$ approaches zero, since in this limit the stop masses become equal and the phase space of the $\tilde{t}_2 \rightarrow \tilde{t}_1 + h$ decay vanishes.

As expected from Eq. (13), the $\tilde{t}_2 \rightarrow \tilde{t}_1 + h$ decay width is quite small ($\lesssim 20 \text{ GeV}$) in the single scale scenario with mass-degenerate stop soft-breaking masses (see the right panel of Fig. 3). If low-mass electroweakinos are present, the $\tilde{t}_2 \rightarrow \tilde{t}_1 + h$ decay width

is unchanged. As a consequence of the small $\tilde{t}_2 \rightarrow \tilde{t}_1 + h$ decay width, the presence of additional decay channels for \tilde{t}_2 (i.e., $\tilde{t}_2 \rightarrow t\tilde{\chi}^0, b\tilde{\chi}^+$), however, suppresses the branching ratio of the $\tilde{t}_2 \rightarrow \tilde{t}_1 + h$ decay channel to values below $\sim 15\%$.

The situation is different if $m_{\tilde{t}_1} \ll m_{\tilde{t}_2}$ (see blue curves in Fig. 3). In this case, the $\tilde{t}_2 \rightarrow \tilde{t}_1 + h$ decay width is significantly larger ($\lesssim 200$ GeV) as expected from Eq. (12). This mass hierarchy, however, also allows large partial decay widths for other decay channels like $\tilde{t}_2 \rightarrow \tilde{t}_1 + Z$. Consequently, $\text{BR}(\tilde{t}_2 \rightarrow \tilde{t}_1 + h)$ reaches only maximal values of $\sim 33\%$ for $\hat{X}_t \sim \pm 3$ in this scenario. In contrast to the case of $m_{\tilde{t}_L} = m_{\tilde{t}_R}$, the presence of low-mass electroweakinos further lowers this branching ratio by only $\lesssim 5\%$, since for $m_{\tilde{t}_1} \ll m_{\tilde{t}_2}$ the partial decay widths of the $\tilde{t}_2 \rightarrow \tilde{t}_1 + h$ decay and the electroweakino decays are similar in size (as expected from Eq. (12)).

In summary, the usefulness of the $\tilde{t}_2 \rightarrow \tilde{t}_1 + h$ process to extract X_t crucially depends on the sparticle mass hierarchy. The presence of additional decay channels or an approximate mass degeneracy between the stop quarks can easily suppress the $\tilde{t}_2 \rightarrow \tilde{t}_1 + h$ branching ratio making it hard to measure it precisely at a future experiment.

3.4. Relation to the mass and the couplings of the SM-like Higgs boson

In view of the discussion above, one might wonder whether for stop masses in the multi-TeV regime the parameter X_t has any significant phenomenological impact at all. However, the situation is very different regarding the impact of the parameter X_t on the prediction for the mass of the SM-like Higgs boson.

While the Higgs-boson mass is a free parameter in the SM, the mass of the SM-like Higgs boson in the MSSM, M_h , can be computed in terms of the model parameters as a consequence of the underlying symmetry (see Ref. [37] for a recent review). M_h is bounded to be below M_Z at the tree level. Loop corrections can, however, increase it to the experimentally measured value of $\simeq 125$ GeV.

The dominant corrections at the one-loop level arise from the stop/top sector and are, in the limit $M_A \gg M_Z$ (M_A being the A boson mass), controlled by the two parameters M_{SUSY} and X_t ,

$$M_h^2 \simeq m_h^2 + 12k \frac{m_t^4}{v^2} \left(\ln \frac{M_{\text{SUSY}}^2}{m_t^2} + |\hat{X}_t|^2 - \frac{1}{12} |\hat{X}_t|^4 \right) + \dots, \quad (14)$$

where $m_h^2 = M_Z^2 c_{2\beta}^2$ is the tree-level mass (again in the limit $M_A \gg M_Z$), M_{SUSY} is the geometric mean of the stop masses, $k \equiv 1/(16\pi^2)$ is the loop factor, and the ellipsis denotes subdominant one-loop and higher-order terms. Apart from M_{SUSY} and t_β (and SM parameters),⁵ only \hat{X}_t strongly influences the dominant one-loop correction. This

⁵The mass scale of the heavy Higgs bosons enters at lowest order and can in principle have a significant impact on the prediction for M_h . Existing search limits in combination with measurements of the properties of the SM-like Higgs boson, however, put strong lower bounds on M_A . Since for $M_A \gg M_Z$ the increase in M_h for rising M_A quickly saturates, in the phenomenologically viable mass region of M_A (see e.g. Refs. [38–40]) the dependence of M_h on M_A is subdominant compared to the dependence on M_{SUSY} and X_t .

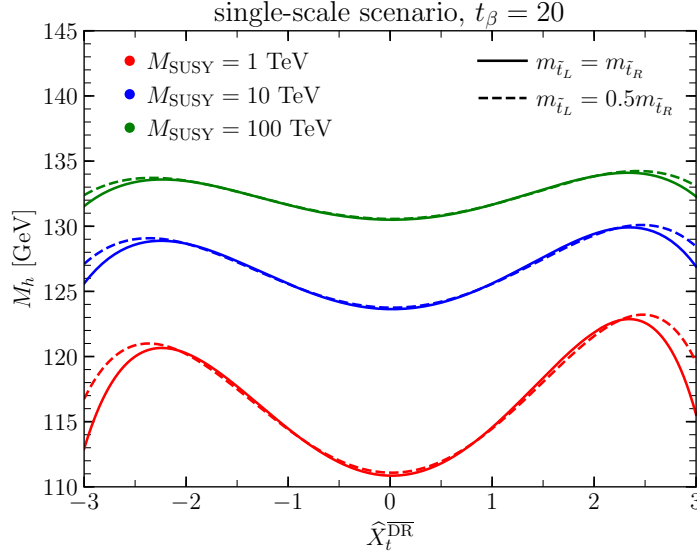


Figure 4: The mass of the SM-like Higgs boson, M_h , as a function of $\hat{X}_t^{\overline{\text{DR}}}$. Results for M_h are shown in a single-scale scenario with $t_\beta = 20$, for two possible choices of the stop soft-SUSY breaking masses, namely $m_{\tilde{t}_L} = m_{\tilde{t}_R}$ (solid curves) and $m_{\tilde{t}_L} = 0.5 m_{\tilde{t}_R}$ (dashed curves), and for three different values of M_{SUSY} : $M_{\text{SUSY}} = 1$ TeV (red), $M_{\text{SUSY}} = 10$ TeV (blue), and $M_{\text{SUSY}} = 100$ TeV (green).

means that if both stops are discovered, the measurement of M_h can be used to determine X_t in the MSSM (under the assumption of a specific t_β value).

This is illustrated in Fig. 4 showing M_h as a function of $\hat{X}_t^{\overline{\text{DR}}}$ for $t_\beta = 20$ (calculated using **FeynHiggs** 2.18.1 [32, 41–48]).⁶ As above, M_{SUSY} is defined to be the geometric mean of the two stop masses. A single-scale scenario is considered, where all soft SUSY-breaking masses (as well as the A boson mass M_A and μ) are chosen to be equal to M_{SUSY} which is set to 1 TeV (red), 10 TeV (blue), and 100 TeV (green). For the solid lines, $m_{\tilde{t}_L} = m_{\tilde{t}_R}$ is set; for the dashed lines, $m_{\tilde{t}_L} = 0.5 m_{\tilde{t}_R}$ is used. For $M_{\text{SUSY}} = 1$ TeV, the prediction for M_h shows a very pronounced dependence on $\hat{X}_t^{\overline{\text{DR}}}$ varying between ~ 111 GeV and ~ 123 GeV within the considered range of $\hat{X}_t^{\overline{\text{DR}}}$.⁷ The sizeable variation of the prediction for M_h with $\hat{X}_t^{\overline{\text{DR}}}$ even for the much higher values for M_{SUSY} of 10 TeV (blue curves) and 100 TeV (green curves) indicates the potential for a precise determination of X_t from the achieved high-precision measurement of M_h (for scenarios where the theoretical prediction is compatible with the experimental value and assuming

⁶**FeynHiggs** computes M_h including the full one-loop corrections as well as the dominant two-loop corrections in the limit of vanishing electroweak gauge couplings. Moreover, leading, next-to-leading, and next-to-next-to-leading logarithmic contributions are resummed using an effective field theory approach. For our numerical analysis, all trilinear couplings (except A_t) are chosen to be zero, and the stop sector is renormalised in the $\overline{\text{DR}}$ scheme (see Section 4.4).

⁷Outside the range $-3 \lesssim \hat{X}_t \lesssim 3$, colour-breaking minima can occur rendering this region in large parts unphysical (see e.g. Refs. [49, 50]).

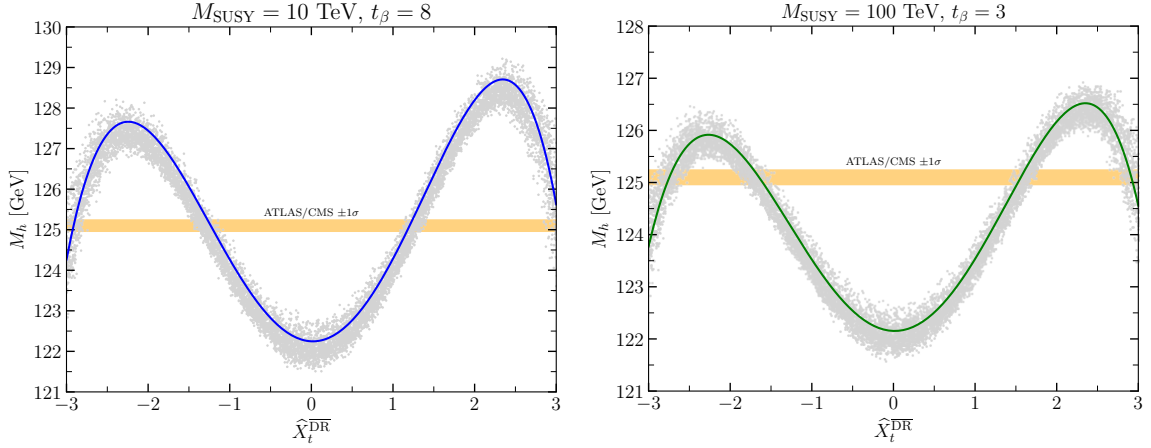


Figure 5: The mass of the SM-like Higgs boson, M_h , as a function of \hat{X}_t . *Left*: The blue curve displays the predicted value of M_h for $t_\beta = 8$ in a single-scale scenario with $M_{\text{SUSY}} = 10$ TeV, where all BSM mass terms are set to M_{SUSY} and all trilinear couplings other than A_t are set to zero. The gray points are obtained by varying the mass parameters and the trilinear couplings randomly in the range $[1/2 M_{\text{SUSY}}, 2 M_{\text{SUSY}}]$. The orange band shows the value of the combined ATLAS/CMS measurement for M_h together with its 1σ uncertainty. *Right*: As for the left plot, but the green curve displays the predicted value of M_h for $t_\beta = 3$ and $M_{\text{SUSY}} = 100$ TeV.

further progress on the reduction of the theoretical uncertainty in the prediction of M_h , which for instance in a scenario in which all BSM particles are close in mass has been estimated to be $\lesssim 1$ GeV, see the discussion in Ref. [51]). Even if the assumption $m_{\tilde{t}_L} = m_{\tilde{t}_R}$ is relaxed and e.g. $m_{\tilde{t}_L} = 0.5 m_{\tilde{t}_R}$ (dashed lines) is chosen, the prediction for M_h only changes significantly for $|\hat{X}_t| \gtrsim 2.5$, showing the robustness of the dependence of M_h on X_t .

These findings are further demonstrated in Fig. 5. In the left panel, we show the dependence of M_h on \hat{X}_t^{DR} for $M_{\text{SUSY}} = 10$ TeV and $t_\beta = 8$ ⁸ (blue curve) in comparison to the current 1σ experimental uncertainty band in orange. The theoretical prediction for M_h as a function of \hat{X}_t^{DR} has the following sources of uncertainties: unknown higher-order corrections, see Ref. [51] for a detailed discussion of the theoretical uncertainty of the Higgs mass calculation implemented in **FeynHiggs**, the experimental errors of the input parameters of the SM, see Ref. [37], and the lacking knowledge of the values of the other SUSY parameters entering the prediction for M_h . In order to illustrate the effect of the latter uncertainty, in addition to the parameter setting of the blue curve, for which all non-SM masses are set equal to M_{SUSY} and all trilinear couplings (apart from A_t) are set to zero, we randomly vary each of these parameters (including all trilinear couplings except A_t , which is fixed via X_t) independently in the interval $[1/2 M_{\text{SUSY}}, 2 M_{\text{SUSY}}]$. In this way, we have produced 10^4 parameter points. They are

⁸Qualitatively similar results are expected for $\tan \beta = 20$, as in Fig. 4.

shown in the form of small grey points in addition to the blue curve. We find that all of these points lie within ~ 0.5 GeV of the single scale scenario. This implies that in a situation where the stop masses and t_β will be known with reasonable accuracy in the future a reliable determination of X_t would be possible from confronting the theoretical prediction for M_h with the experimental value even if the information about the other parts of the SUSY spectrum is very limited (see also discussion in Ref. [13]). A similar approach that semi-analytically expresses the stop trilinear coupling in terms of M_h has recently been discussed in Ref. [14].

The right panel of Fig. 5 displays the remarkable feature that an indirect determination of X_t from M_h can even be achieved for a SUSY scale as high as $M_{\text{SUSY}} = 100$ TeV. The green curve shows the prediction for M_h for $M_{\text{SUSY}} = 100$ TeV and $t_\beta = 3$. As in the left plot, the small grey points show the random variations of the SUSY parameters in the interval $[1/2 M_{\text{SUSY}}, 2 M_{\text{SUSY}}]$. The fact that the prediction for M_h has a high sensitivity to the ratio X_t/M_{SUSY} even for the case where the SUSY scale is so high that it may be beyond the reach of any future collider clearly shows the unique role of the prediction for the SM-like Higgs mass in constraining the stop mixing parameter X_t (of course, from the information about M_h alone X_t cannot be fully determined).

While only the prediction for the mass of the SM-like Higgs boson shows the special feature that it has a high sensitivity to X_t/M_{SUSY} even for very high values of M_{SUSY} , the effects of varying X_t on the couplings of the SM-like Higgs boson tend to vanish in the decoupling region where M_{SUSY} is large. On the other hand, for relatively low SUSY scales also high-precision measurements of the branching ratios of the SM-like Higgs boson can provide supplementary information on X_t . Exploratory studies addressing the sensitivity of Higgs branching ratios to X_t have been carried out in Refs. [11, 12].

4. Renormalisation of the stop sector

Based on the discussion of the various approaches to determine X_t from physical observables, we compare in this Section different renormalisation schemes for the top/stop sector.

Working for simplicity in the limit of vanishing electroweak gauge coupling, we renormalise the parameters appearing in the stop mass matrix (see Eq. (1)) as follows,⁹

$$\begin{aligned} m_{\tilde{t}_{L/R}}^2 &\rightarrow m_{\tilde{t}_{L/R}}^2 + \delta^{(1)} m_{\tilde{t}_{L/R}}^2, \\ X_t &\rightarrow X_t + \delta^{(1)} X_t, \\ m_t &\rightarrow m_t + \delta^{(1)} m_t. \end{aligned} \tag{15}$$

In this way the stop mass matrix $\mathbf{M}_{\tilde{t}}$ acquires the counterterm

$$\delta^{(1)} \mathbf{M}_{\tilde{t}} = \begin{pmatrix} \delta^{(1)} m_{\tilde{t}_L}^2 + \delta^{(1)} m_t^2 & X_t^* \delta^{(1)} m_t + m_t \delta^{(1)} X_t^* \\ X_t \delta^{(1)} m_t + m_t \delta^{(1)} X_t & \delta^{(1)} m_{\tilde{t}_R}^2 + \delta^{(1)} m_t^2 \end{pmatrix}. \tag{16}$$

⁹See Refs. [27, 29–31] for a detailed discussion, employing similar notations, of the renormalisation scheme presented in this Section. Further discussions of the renormalisation of the stop/top sector can be found in Refs. [15–26, 28].

Using the tree-level transformation matrix $\mathbf{U}_{\tilde{t}}$, which relates gauge and mass eigenstates (see Eq. (2)), we define

$$\mathbf{U}_{\tilde{t}} \delta^{(1)} \mathbf{M}_{\tilde{t}} \mathbf{U}_{\tilde{t}}^\dagger = \begin{pmatrix} \delta^{(1)} m_{\tilde{t}_1}^2 & \delta^{(1)} m_{\tilde{t}_{12}}^2 \\ \delta^{(1)} m_{\tilde{t}_{21}}^2 & \delta^{(1)} m_{\tilde{t}_2}^2 \end{pmatrix}, \quad (17)$$

where $\delta^{(1)} m_{\tilde{t}_{21}}^2 = (\delta^{(1)} m_{\tilde{t}_{12}}^2)^*$.

Rotating back to the gauge-eigenstate basis, the counterterms for the soft-breaking parameters read,

$$\begin{aligned} \delta^{(1)} X_t &= \frac{1}{m_t} [\mathbf{U}_{\tilde{t}_{11}} \mathbf{U}_{\tilde{t}_{12}}^* (\delta^{(1)} m_{\tilde{t}_1}^2 - \delta^{(1)} m_{\tilde{t}_2}^2) \\ &\quad + \delta^{(1)} m_{\tilde{t}_{12}}^2 \mathbf{U}_{\tilde{t}_{21}} \mathbf{U}_{\tilde{t}_{12}}^* + \delta^{(1)} m_{\tilde{t}_{21}}^2 \mathbf{U}_{\tilde{t}_{11}} \mathbf{U}_{\tilde{t}_{22}}^* - X_t \delta^{(1)} m_t], \end{aligned} \quad (18a)$$

$$\begin{aligned} \delta^{(1)} m_{\tilde{t}_L}^2 &= \delta^{(1)} m_{\tilde{t}_1}^2 |\mathbf{U}_{\tilde{t}_{11}}|^2 + \delta^{(1)} m_{\tilde{t}_2}^2 |\mathbf{U}_{\tilde{t}_{12}}|^2 \\ &\quad + \delta^{(1)} m_{\tilde{t}_{12}}^2 \mathbf{U}_{\tilde{t}_{21}} \mathbf{U}_{\tilde{t}_{11}}^* + \delta^{(1)} m_{\tilde{t}_{21}}^2 \mathbf{U}_{\tilde{t}_{11}} \mathbf{U}_{\tilde{t}_{22}}^* - 2m_t \delta^{(1)} m_t, \end{aligned} \quad (18b)$$

$$\begin{aligned} \delta^{(1)} m_{\tilde{t}_R}^2 &= \delta^{(1)} m_{\tilde{t}_1}^2 |\mathbf{U}_{\tilde{t}_{12}}|^2 + \delta^{(1)} m_{\tilde{t}_2}^2 |\mathbf{U}_{\tilde{t}_{22}}|^2 \\ &\quad + \delta^{(1)} m_{\tilde{t}_{12}}^2 \mathbf{U}_{\tilde{t}_{22}} \mathbf{U}_{\tilde{t}_{12}}^* + \delta^{(1)} m_{\tilde{t}_{21}}^2 \mathbf{U}_{\tilde{t}_{12}} \mathbf{U}_{\tilde{t}_{22}}^* - 2m_t \delta^{(1)} m_t. \end{aligned} \quad (18c)$$

At this point, a remark should be made about the renormalisation of the off-diagonal entries of the matrix $\mathbf{M}_{\tilde{t}}$. We have used X_t as a free parameter, while the entries of the transformation matrix $\mathbf{U}_{\tilde{t}}$ were set to their tree-level values. Sometimes, a slightly different approach is used [25]. Namely, instead of renormalising the X_t parameter, the angle $\theta_{\tilde{t}}$ and the phase ϕ_{X_t} of the rotation matrix $\mathbf{U}_{\tilde{t}}$ are renormalised,

$$\theta_{\tilde{t}} \rightarrow \theta_{\tilde{t}} + \delta^{(1)} \theta_{\tilde{t}}, \quad \phi_{X_t} \rightarrow \phi_{X_t} + \delta^{(1)} \phi_{X_t}. \quad (19)$$

At the first step, the original mass matrix is expressed in terms of $\theta_{\tilde{t}}$ and ϕ_{X_t} as,

$$\mathbf{M}_{\tilde{t}} = \begin{pmatrix} \cos^2 \theta_{\tilde{t}} m_{\tilde{t}_1}^2 + \sin^2 \theta_{\tilde{t}} m_{\tilde{t}_2}^2 & (m_{\tilde{t}_1}^2 - m_{\tilde{t}_2}^2) \sin \theta_{\tilde{t}} \cos \theta_{\tilde{t}} e^{-i\phi_{X_t}} \\ (m_{\tilde{t}_1}^2 - m_{\tilde{t}_2}^2) \sin \theta_{\tilde{t}} \cos \theta_{\tilde{t}} e^{i\phi_{X_t}} & \cos^2 \theta_{\tilde{t}} m_{\tilde{t}_2}^2 + \sin^2 \theta_{\tilde{t}} m_{\tilde{t}_1}^2 \end{pmatrix}. \quad (20)$$

Using the definition of the counterterms, given in Eq. (18), the counterterms for the entries of the original mass matrix can then be written as,

$$\delta^{(1)} \mathbf{M}_{\tilde{t}_{11}} = \cos^2 \theta_{\tilde{t}} \delta^{(1)} m_{\tilde{t}_1}^2 + \sin^2 \theta_{\tilde{t}} \delta^{(1)} m_{\tilde{t}_2}^2 + (m_{\tilde{t}_2}^2 - m_{\tilde{t}_1}^2) \sin 2\theta_{\tilde{t}} \delta^{(1)} \theta_{\tilde{t}}, \quad (21a)$$

$$\begin{aligned} \delta^{(1)} \mathbf{M}_{\tilde{t}_{12}} &= (\delta^{(1)} m_{\tilde{t}_1}^2 - \delta^{(1)} m_{\tilde{t}_2}^2) \sin \theta_{\tilde{t}} \cos \theta_{\tilde{t}} e^{-i\phi_{X_t}} \\ &\quad + (m_{\tilde{t}_1}^2 - m_{\tilde{t}_2}^2) (\delta^{(1)} \theta_{\tilde{t}} \cos 2\theta_{\tilde{t}} - i\delta^{(1)} \phi_{X_t} \sin \theta_{\tilde{t}} \cos \theta_{\tilde{t}}) e^{-i\phi_{X_t}}, \end{aligned} \quad (21b)$$

$$\begin{aligned} \delta^{(1)} \mathbf{M}_{\tilde{t}_{21}} &= (\delta^{(1)} m_{\tilde{t}_1}^2 - \delta^{(1)} m_{\tilde{t}_2}^2) \sin \theta_{\tilde{t}} \cos \theta_{\tilde{t}} e^{i\phi_{X_t}} \\ &\quad + (m_{\tilde{t}_1}^2 - m_{\tilde{t}_2}^2) (\delta^{(1)} \theta_{\tilde{t}} \cos 2\theta_{\tilde{t}} + i\delta^{(1)} \phi_{X_t} \sin \theta_{\tilde{t}} \cos \theta_{\tilde{t}}) e^{i\phi_{X_t}}, \end{aligned} \quad (21c)$$

$$\delta^{(1)} \mathbf{M}_{\tilde{t}_{22}} = \cos^2 \theta_{\tilde{t}} \delta^{(1)} m_{\tilde{t}_2}^2 + \sin^2 \theta_{\tilde{t}} \delta^{(1)} m_{\tilde{t}_1}^2 + (m_{\tilde{t}_1}^2 - m_{\tilde{t}_2}^2) \sin 2\theta_{\tilde{t}} \delta^{(1)} \theta_{\tilde{t}}. \quad (21d)$$

By transforming the counterterm matrix, $\delta^{(1)} \mathbf{M}_{\tilde{t}}$, to the mass eigenstates basis, we arrive at the following expression,

$$\delta^{(1)} m_{\tilde{t}_{12}}^2 = e^{-i\phi_{X_t}} (m_{\tilde{t}_1}^2 - m_{\tilde{t}_2}^2) (\delta^{(1)} \theta_{\tilde{t}} - i\delta^{(1)} \phi_{X_t} \sin \theta_{\tilde{t}} \cos \theta_{\tilde{t}}), \quad (22)$$

which relates the off-diagonal stop mass matrix counterterm to the stop mixing angle and stop phase counterterms.

4.1. $\overline{\text{DR}}$ scheme

From a technical point of view, renormalising the stop masses and X_t in the $\overline{\text{DR}}$ scheme is easiest. In this scheme, the stop masses and X_t are, however, renormalisation scale dependent quantities and have no direct relation to physical observables. On the other hand, a renormalisation in the $\overline{\text{DR}}$ scheme can be advantageous if high-scale SUSY-breaking models are studied. These models impose boundary conditions at some high scale on the $\overline{\text{DR}}$ parameters. Renormalisation group running is then used to evolve the parameters to the low scale, where physical observables are calculated.

4.2. Process-dependent OS scheme

The stop sector can also be renormalised in the OS scheme. This is straightforward for the stop masses, which then correspond to the respective physical masses. To achieve this the counterterms for the diagonal elements of the stop matrix, $m_{\tilde{t}_1}^2$ and $m_{\tilde{t}_2}^2$, are fixed via the on-shell conditions,

$$\delta^{(1)}m_{\tilde{t}_1}^2 = \text{Re } \Sigma_{\tilde{t}_1\tilde{t}_1}^{(1)}(m_{\tilde{t}_1}^2), \quad \delta^{(1)}m_{\tilde{t}_2}^2 = \text{Re } \Sigma_{\tilde{t}_2\tilde{t}_2}^{(1)}(m_{\tilde{t}_2}^2), \quad (23)$$

where $\Sigma_{\tilde{t}_i\tilde{t}_i}^{(1)}$ is the one-loop $\tilde{t}_i\tilde{t}_i$ self energy. Note that if we were also including the sbottom sector in this discussion, it would not be possible to renormalise all four stop and sbottom masses on-shell, as a consequence of an $SU(2)_L$ relation — see e.g. the discussion in Ref. [18].

It is much more difficult to connect the stop mixing parameter to a physical process. An obvious candidate is the decay process $\tilde{t}_2 \rightarrow \tilde{t}_1 + h$, which depends on X_t at the tree level. As discussed in Section 3, the decay rate and therefore the prospects for experimentally observing this process are, however, highly dependent on the sparticle mass spectrum. In parameter scans this implies that an OS definition of X_t via the process $\tilde{t}_2 \rightarrow \tilde{t}_1 + h$ will only be usable for certain parts of the parameter space. The same holds also for processes involving the stop mixing angle at the tree level (see again Section 3). Other processes involving a stop–stop–Higgs coupling at the tree level are experimentally difficult to access (e.g. $\tilde{t}_1\tilde{t}_2 \rightarrow h$).

4.3. Process-independent OS scheme

Because of the difficulties in defining a process-dependent OS scheme for X_t , a process-independent OS scheme is often used in the literature (see e.g. Refs. [21, 24, 25, 27, 29]).

The counterterm for the off-diagonal entry of the stop mass matrix is fixed via a symmetric on-shell condition,

$$\delta^{(1)}m_{\tilde{t}_{12}}^2 = \frac{1}{2} \text{Re } \left[\Sigma_{\tilde{t}_1\tilde{t}_2}^{(1)}(m_{\tilde{t}_1}^2) + \Sigma_{\tilde{t}_1\tilde{t}_2}^{(1)}(m_{\tilde{t}_2}^2) \right]. \quad (24)$$

The counterterms $\delta^{(1)}X_t$ or $\delta^{(1)}\theta_{\tilde{t}}$ can then be obtained using the expressions in Eqs. (18a) to (18c).

In MSSM scenarios without \mathcal{CP} -violation in the stop sector, the expression for $\delta^{(1)}\theta_{\tilde{t}}$ reduces to

$$\delta^{(1)}\theta_{\tilde{t}} = \frac{\text{Re } \Sigma_{\tilde{t}_1\tilde{t}_2}^{(1)}(m_{\tilde{t}_1}^2) + \text{Re } \Sigma_{\tilde{t}_1\tilde{t}_2}^{(1)}(m_{\tilde{t}_2}^2)}{2(m_{\tilde{t}_1}^2 - m_{\tilde{t}_2}^2)}, \quad (25)$$

which has been used in Refs. [23, 52–55].

The disadvantage of such a scheme, where the counterterms are defined in terms of off-diagonal self-energies at a certain value of the squared external momentum, is that the parameters defined in this way are not directly related to physical observables. In fact, the counterterms defined in Eqs. (24) and (25) will in general be gauge-dependent.

4.4. $\overline{\text{MDR}}$ and $\overline{\text{DR}}$ scheme

Besides the possibility to connect the parameters to physical observables (which is difficult for the stop mixing parameter as discussed above), the OS scheme has a further advantage with respect to the $\overline{\text{DR}}$ scheme: it ensures the proper decoupling of the gluino. While in the $\overline{\text{DR}}$ scheme quantum corrections proportional to powers of the gluino mass appear [53], these are absent in the OS scheme leaving only a logarithmic dependence on the gluino mass if the gluino mass is much larger than the stop masses. This issue has been discussed in Refs. [42, 51, 53, 56–62].

As an alternative to using the OS scheme, the $\overline{\text{DR}}$ scheme can be modified in order to absorb the corrections enhanced by powers of the gluino mass into the definition of the parameters,

$$\begin{aligned} \left(m_{\tilde{t}_{L,R}}^{\overline{\text{MDR}}}\right)^2(Q) &= \left(m_{\tilde{t}_{L,R}}^{\overline{\text{DR}}}\right)^2(Q) \left[1 + \frac{\alpha_s}{\pi} C_F \frac{|M_3|^2}{m_{\tilde{t}_{L,R}}^2} \left(1 + \ln \frac{Q^2}{|M_3|^2}\right)\right], \\ X_t^{\overline{\text{MDR}}}(Q) &= X_t^{\overline{\text{DR}}}(Q) - \frac{\alpha_s}{\pi} C_F M_3 \left(1 + \ln \frac{Q^2}{|M_3|^2}\right), \end{aligned} \quad (26)$$

where $\alpha_s \equiv g_3^2/(4\pi)$. As discussed in Ref. [62], this $\overline{\text{MDR}}$ scheme consistently avoids the occurrence of terms enhanced by powers of the gluino mass and ensures a proper decoupling behaviour in the limit where the gluino is much heavier than the stops.

4.5. Mixed schemes

As an alternative of using a pure OS or a pure $\overline{\text{DR}}/\overline{\text{MDR}}$ scheme, the different schemes can also be mixed in the sense that e.g. the stop masses are renormalised in the OS scheme while the stop mixing parameter is renormalised in the $\overline{\text{DR}}/\overline{\text{MDR}}$ scheme. This particular scheme has the advantage that the stop masses closely correspond to the physical masses while the stop mixing parameter, which is difficult to connect to a physical observable, is renormalised in a simple process-independent scheme.

We stress however that mixed schemes have the disadvantage of the potential occurrence of uncancelled ϵ^1 parts of loop integrals (ϵ being the UV regulator introduced in dimensional regularisation/reduction). In pure $\overline{\text{MS}}/\overline{\text{DR}}$ and OS schemes, all ϵ^1 parts of the involved loop integrals cancel in the final result. For mixed schemes, this is, however, not necessarily the case as noted e.g. in Refs. [63, 64]. This happens for mixed schemes where a quantity is renormalized in the $\overline{\text{MS}}/\overline{\text{DR}}$ scheme at the two-loop level but receives a contribution from a one-loop OS counterterm in a sub-loop.

If ϵ^1 parts of loop integrals remain in the final result, the input parameters cannot simply be converted from one scheme to another. For example, a pure $\overline{\text{MS}}/\overline{\text{DR}}$ calculation cannot easily be transferred to a calculation in the mixed scheme by a conversion of the input parameter since the $\overline{\text{MS}}/\overline{\text{DR}}$ calculation does not contain any ϵ^1 parts of loop integrals and these also cannot be generated by a conversion (without prior knowledge of the structure of the calculations; for examples of a conversion including the ϵ^1 pieces, see e.g. Refs. [63, 65]). Moreover, the occurrence of uncancelled ϵ^1 parts of loop integrals implies that $\overline{\text{MS}}/\overline{\text{DR}}$ parameters in a mixed scheme have a different meaning than the corresponding $\overline{\text{MS}}/\overline{\text{DR}}$ parameters in a pure $\overline{\text{MS}}/\overline{\text{DR}}$ calculation.

Concerning the scheme where the stop mixing parameter is renormalised in the $\overline{\text{DR}}$ or $\overline{\text{MDR}}$ scheme and the stop masses in the OS scheme, we note that uncancelled ϵ^1 parts of loop integrals affecting the definition of X_t will only appear for calculations where the stop sector needs to be renormalised at the two-loop level. Only in this case would a one-loop OS counterterm yield a sub-loop contribution to the two-loop $\overline{\text{DR}}/\overline{\text{MDR}}$ renormalisation of X_t . Thus, in the predictions of the Higgs boson masses this issue of uncancelled ϵ^1 terms will first appear at the three-loop level.

5. Renormalisation of the stop mixing parameter and the prediction for the mass of the SM-like Higgs boson

Our discussion in Section 3 led to the conclusion that confronting the prediction for the mass of the SM-like Higgs boson with the measured experimental value offers the best prospects for determining the stop mixing parameter. Consequently, an appropriate renormalisation scheme for X_t should be such that a precise Higgs mass prediction can be derived. We start with a discussion of the use of the process-independent OS scheme.

Different methods are employed in precise calculations of the mass of the SM-like Higgs boson. In the fixed-order approach, loop corrections to the inverse Higgs propagator matrix are calculated within the full MSSM. In this framework, a process-independent OS scheme is straightforward to implement. While this approach is suitable for stop masses below or around the TeV scale, its achieved accuracy suffers from the appearance of large logarithmic corrections increasing the size of unknown higher-order corrections for stop masses above the TeV scale. These large logarithmic contributions can be resummed in an EFT approach. In its simplest form, all non-SM particles are integrated out a common mass scale, which is typically set to M_{SUSY} . For the calculation of the

threshold corrections between the low-energy EFT (e.g. the SM) and the high-energy MSSM, typically the limit $v/M_{\text{SUSY}} \rightarrow 0$ is taken, neglecting all higher-order operators appearing in the EFT.¹⁰ For this reason, the EFT calculation is expected to have a lower accuracy for low SUSY scales. Using an OS definition for X_t in the calculation of the threshold corrections would induce large logarithmic terms $\sim \ln M_{\text{SUSY}}^2/m_t^2$ into the threshold corrections spoiling the underlying assumption of the EFT approach. For this reason, EFT calculations typically employ the $\overline{\text{DR}}$ scheme (or the $\overline{\text{MDR}}$ scheme) for the renormalisation of X_t .

If X_t could be extracted from a physical observable different from the mass of the SM-like Higgs boson, one would need to extract the input parameter for the EFT calculation of M_h — $X_t^{\overline{\text{DR}}}$ or $(X_t^{\overline{\text{MDR}}})$ — from the physical observable. For simplicity we assume here that this observable is closely related to the process-independent X_t^{OS} . It is well-known that in the relation between the OS and the $\overline{\text{DR}}$ definition of X_t large unresummed logarithms can appear in the limit $v/M_{\text{SUSY}} \rightarrow 0$.

The same issue arises in the hybrid calculations combining the fixed-order and the EFT approach in order to obtain a precise M_h prediction for low and high SUSY scales. While the OS scheme can easily be used in the fixed-order part of the calculation, the fixed-order OS quantities have to be converted to $\overline{\text{DR}}$ (or $\overline{\text{MDR}}$) quantities as input for the EFT calculation. This poses the question of whether the logarithms appearing in the relation between X_t^{OS} and $X_t^{\overline{\text{DR}}}$ can be resummed.

The relation between the OS and the $\overline{\text{DR}}$ scheme for X_t can be written as follows,

$$X_t^{\text{OS}} = X_t^{\overline{\text{DR}}}(M_{\text{SUSY}}) \frac{m_t^{\overline{\text{DR}},\text{MSSM}}(M_{\text{SUSY}})}{m_t^{\text{OS}}} - \frac{1}{m_t^{\text{OS}}} \delta^{(1)}(m_t X_t) \Big|_{\text{fin}}. \quad (27)$$

We are especially interested in large logarithms appearing in this relation between X_t^{OS} and $X_t^{\overline{\text{DR}}}$, since such logarithms can potentially spoil the precision of the overall calculation. Both terms on the right-hand side of the Eq. (27) can contain large logarithms, but these logarithms are of a different origin.

Let us start our discussion with the first term. The relation between the OS and the $\overline{\text{DR}}$ running top mass can be derived by

$$m_t^{\overline{\text{DR}},\text{MSSM}}(M_{\text{SUSY}}) = m_t^{\text{OS}} + \delta^{(1)} m_t^{\text{OS}} \Big|_{\text{fin}}, \quad (28)$$

where the finite counterterm has to be evaluated at the renormalisation scale $Q = M_{\text{SUSY}}$. The finite part of the OS counterterm of the top-quark mass will contain terms like $\ln Q^2/m_t^2$. Since $Q = M_{\text{SUSY}}$, these terms give rise to large logarithms. The described procedure yields,

$$(\delta^{(1)} m_t^{\text{OS}}) \Big|_{\text{fin}}^{Q=M_{\text{SUSY}}} = m_t^{\text{OS}} \left[- \left(\frac{\alpha_s}{\pi} - \frac{3\alpha_t}{16\pi} \right) \ln \frac{M_{\text{SUSY}}^2}{m_t^2} + \text{non-log} \right] + \dots, \quad (29)$$

¹⁰See also Ref. [66] for a departure from this assumption. In this work, the impact of dimension-6 operators to the calculation of the Higgs mass when matching the MSSM onto the SM was considered, and found to be moderate.

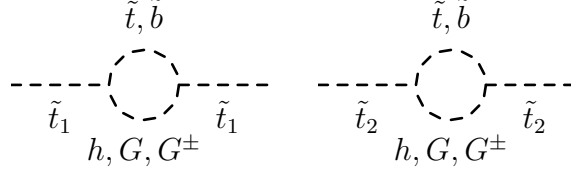


Figure 6: Feynman diagrams generating the large logarithms in Eq. (31).

where $\alpha_t \equiv y_t^2/(4\pi) = h_t^2/(4\pi s_\beta^2)$ and “non-log” is used as a placeholder for terms which do not contain large logarithms, but can contain “small logarithms,” i.e. logarithms of the ratios m_A/M_{SUSY} , $|M_3|/M_{\text{SUSY}}$, $|\mu|/M_{\text{SUSY}}$. The ellipsis denotes terms that are not proportional to α_s or α_t , and which are numerically less important. Expressions containing additional bottom-Yukawa corrections can be found in Appendix A. The large logarithms of the form $\ln M_{\text{SUSY}}^2/m_t^2$ can be resummed by using the top mass defined in the $\overline{\text{MS}}$ or the $\overline{\text{DR}}$ scheme at M_{SUSY} either in the full MSSM or in the SM.

Now let us proceed with the second term in Eq. (27). We will now demonstrate that this term contains large logarithms if the soft-breaking masses of the stops are degenerate,

$$m_{\tilde{t}_L} = m_{\tilde{t}_R} = M_{\text{SUSY}}. \quad (30)$$

Explicit evaluation of the counterterm $\delta^{(1)}(m_t X_t)|_{\text{fin}}$ in this case shows that it contains the following terms in the limit $M_{\text{SUSY}} \gg m_t$,

$$\delta^{(1)}(m_t X_t)|_{\text{fin}} = \frac{3\alpha_t}{16\pi} m_t X_t |\hat{X}_t|^2 \ln \frac{M_{\text{SUSY}}^2}{m_t^2} + \text{non-log}, \quad (31)$$

where $\hat{X}_t = X_t/M_{\text{SUSY}}$.

The large logarithm in Eq. (31) arise from diagrams involving the Goldstone bosons (see Fig. 6).¹¹ Note that these expressions do not depend on the renormalisation scale. Consequently, these large logarithms have a different origin than the logarithms in Eq. (29).

In Ref. [5], these logarithms have been linked to infrared singularities originating from external-leg corrections. In the present case, the counterterm for the stop mixing angle (see Eq. (25)) is of the same form as a \tilde{t}_1 – \tilde{t}_2 external leg mixing correction relevant for any process involving an external stop quark. As discussed in detail in Ref. [5], an infrared divergence appears in the limit $m_{\tilde{t}_1} \rightarrow m_{\tilde{t}_2}$, which is cured by including Higgs-boson real radiation (note that in the limit $v/M_{\text{SUSY}} \rightarrow 0$, the Higgs boson is massless at the tree level). For a finite mass difference, $\Delta m_t^2 = m_{\tilde{t}_2}^2 - m_{\tilde{t}_1}^2 = 2m_t |X_t|$, this infrared limit is manifest in the form of renormalisation scale independent logarithms involving Δm^2 ,

$$\ln \frac{\Delta m^2}{M_{\text{SUSY}}^2} = \ln 2 + \ln \hat{X}_t - \frac{1}{2} \ln \frac{M_{\text{SUSY}}^2}{m_t^2}, \quad (32)$$

¹¹The counterterms $\delta^{(1)}m_{\tilde{t}_{12}}^2$ and $\delta^{(1)}m_{\tilde{t}_{21}}^2$ do not give rise to the large logarithms in Eq. (31).

which are in direct correspondence to the logarithms of Eq. (31). These logarithms cannot be resummed by integrating out heavy particles (i.e., the stops in the present case), since they originate from the wave-function normalisation of a heavy particle. Moreover, a dangerous enhancement of the logarithmic terms can also occur due to the trilinear couplings contained in their prefactor, X_t in Eq. (31), which can be large. While a resummation can potentially be achieved within the framework of soft-collinear effective field theory, an explicit two-loop calculation in Ref. [5] has shown that logarithmic corrections beyond the one-loop order are expected to be relatively small.

The size of unknown higher-order corrections is, however, not the only concern regarding the conversion of X_t from the OS to the $\overline{\text{DR}}$ scheme. Besides the case of degenerate soft SUSY-breaking masses, of course also the case of non-degenerate soft SUSY-breaking masses needs to be considered. Expanding in powers of v/M_{SUSY} while keeping $m_{\tilde{t}_L} \neq m_{\tilde{t}_R}$, we obtain

$$\delta^{(1)}(m_t X_t)|_{\text{fin}} = \frac{\alpha_t}{8\pi} m_t X_t |\hat{X}_t|^2 \left(\frac{2m_{\tilde{t}_L}}{m_{\tilde{t}_R}} \ln \frac{m_{\tilde{t}_L}^2}{|m_{\tilde{t}_L}^2 - m_{\tilde{t}_R}^2|} + \frac{m_{\tilde{t}_R}}{m_{\tilde{t}_L}} \ln \frac{m_{\tilde{t}_R}^2}{|m_{\tilde{t}_L}^2 - m_{\tilde{t}_R}^2|} \right), \quad (33)$$

where in this case \hat{X}_t is defined as $\hat{X}_t = X_t / \sqrt{m_{\tilde{t}_L} m_{\tilde{t}_R}}$. We note that contrary to the expression given in Eq. (31), this expression does not contain any large logarithms of the form $\ln M_{\text{SUSY}}^2/m_t^2$. In the present case, the mass difference Δm_t^2 regulating the infrared singularity appearing in the wave-function normalisation of the stops is equal to $m_{\tilde{t}_L}^2 - m_{\tilde{t}_R}^2$ — the additional term $2m_t |X_t|$ in the stop mass difference Δm_t^2 can be neglected here in the limit $v/M_{\text{SUSY}} \rightarrow 0$.

To summarise, the conversion formula for the stop mixing parameter X_t in the heavy SUSY limit — $v/M_{\text{SUSY}} \rightarrow 0$ — for the case of the scenario with degenerate squark soft-breaking masses reads,

$$X_t^{\overline{\text{DR}}}(M_{\text{SUSY}}) \Big|_{m_{\tilde{t}_L}=m_{\tilde{t}_R}} = X_t^{\text{OS}} \left\{ 1 + \left[\frac{\alpha_s}{\pi} - \frac{3\alpha_t}{16\pi} \left(1 - \frac{|X_t|^2}{M_{\text{SUSY}}^2} \right) \right] \ln \frac{M_{\text{SUSY}}^2}{m_t^2} \right\} + \text{non-log.} \quad (34)$$

For the case where the stop soft-breaking masses are non-degenerate, the corresponding formula takes the form,

$$X_t^{\overline{\text{DR}}}(M_{\text{SUSY}}) \Big|_{m_{\tilde{t}_L} \neq m_{\tilde{t}_R}} = X_t^{\text{OS}} \left\{ 1 + \left[\frac{\alpha_s}{\pi} - \frac{3\alpha_t}{16\pi} \right] \ln \frac{M_{\text{SUSY}}^2}{m_t^2} \right\} + \text{non-log.} \quad (35)$$

This clearly shows that in the limit $v/M_{\text{SUSY}} \rightarrow 0$ no smooth transition between the cases $m_{\tilde{t}_R} = m_{\tilde{t}_L}$ and $m_{\tilde{t}_R} \neq m_{\tilde{t}_L}$ exists.

The formula that is not expanded in the limit $v/M_{\text{SUSY}} \rightarrow 0$ does not show this behaviour. To illustrate this, we consider a MSSM scenario in which $\mu = 10$ TeV, all soft-breaking masses except for $m_{\tilde{t}_R}$ are equal to $M_{\text{SUSY}} = 10$ TeV, the stop mixing parameter equals $X_t = M_{\text{SUSY}}$, and $\tan \beta = 10$. In Fig. 7, we show the behaviour of the counterterm $\delta^{(1)}(m_t X_t)$, normalised by the top mass m_t and the soft mass $m_{\tilde{t}_L}$,

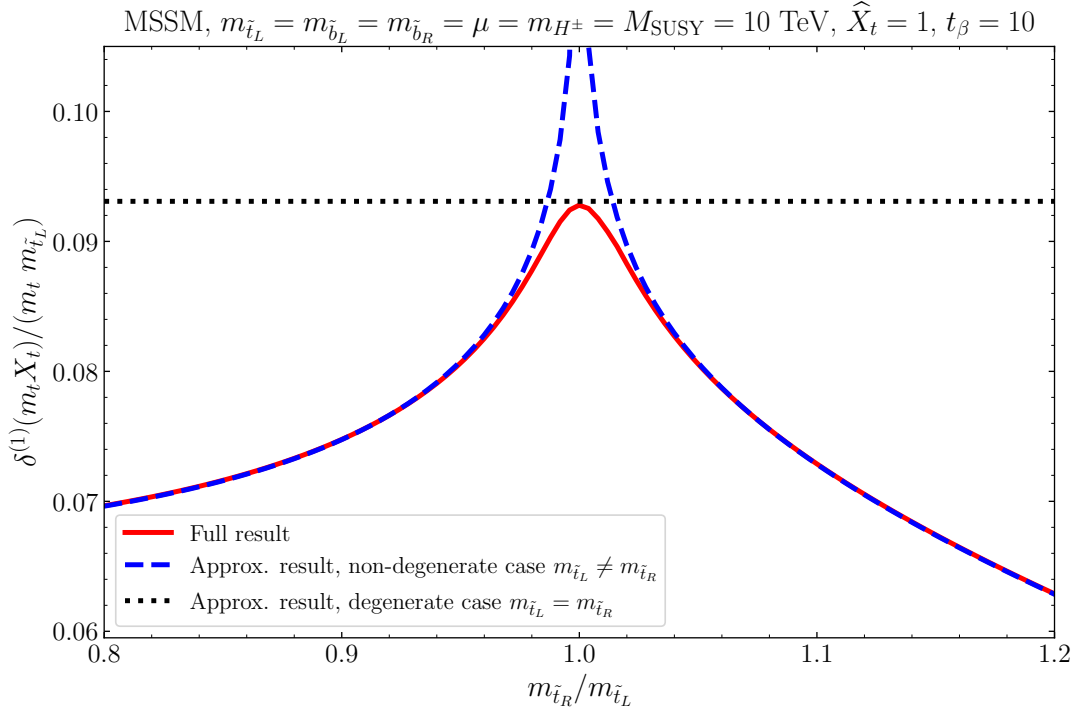


Figure 7: Numerical comparison of $\delta^{(1)}(m_t X_t) / (m_t m_{\tilde{t}_L})$ calculated without any expansion (red solid), calculated in the limit $v/M_{\text{SUSY}} \rightarrow 0$ and $m_{\tilde{t}_L} \neq m_{\tilde{t}_R}$ (blue dashed), as well as calculated in the limit $v/M_{\text{SUSY}} \rightarrow 0$ and $m_{\tilde{t}_L} = m_{\tilde{t}_R}$ (black dotted).

neglecting corrections proportional to the bottom Yukawa and the strong gauge coupling for simplicity.

The solid red curve corresponds to the full expression of the order $\mathcal{O}(\alpha_t)$ contribution to $\delta^{(1)}(m_t X_t)/(m_t m_{\tilde{t}_L})$. The horizontal black dotted line indicates the value corresponding to the approximate expression in Eq. (31), while the blue dashed curve shows the behaviour of Eq. (33). Since the SUSY scale is much heavier than the EW scale, the blue dashed curve yields a good approximation of the behaviour of the red curve for $|m_{\tilde{t}_R}/m_{\tilde{t}_L} - 1| \gtrsim 0.05$. On the other hand it starts to deviate from the red one for values of $m_{\tilde{t}_R}/m_{\tilde{t}_L}$ close to one, and for $m_{\tilde{t}_R}/m_{\tilde{t}_L} = 1$ its value is not defined. At this point the full expression is well approximated by the result that is indicated by the black dotted line.

The one-loop contribution to the counterterm $\delta^{(1)}(m_t X_t)$ proportional to the strong gauge coupling does not exhibit the behaviour described above. More specifically, there is no large logarithm emerging in the $\mathcal{O}(\alpha_s)$ expression for $\delta^{(1)}(m_t X_t)|_{\text{fin}}$ in the heavy SUSY limit regardless whether the squark soft-breaking masses are degenerate or non-degenerate. Furthermore, for the corrections of order $\mathcal{O}(\alpha_s)$ a smooth transition between the two mentioned scenarios exists (since the particles appearing in the loop are fermions or gauge bosons and not scalars).

While it is possible to use the full unexpanded $X_t^{\text{OS}} \rightarrow X_t^{\overline{\text{DR}}}$ conversion, this would mix different orders in the EFT expansion. For this reason and since M_h is the most promising observable to determine X_t (as discussed in Section 3), it seems preferable to use a $\overline{\text{DR}}$ renormalisation of X_t in the fixed-order calculation as well. If an extraction of X_t from another observable than M_h is found to be possible in the future, the issues of large logarithmic contributions to the extraction will, however, reappear. Furthermore, as discussed above, a full $\overline{\text{DR}}$ scheme is problematic because of non-decoupling effects for the case where the gluino is much heavier than the stops, while a mixed scheme where X_t is renormalised in the $\overline{\text{DR}}$ scheme and the stop masses are renormalised in the OS scheme can lead to complications at higher orders because of uncanceled terms of $\mathcal{O}(\epsilon^1)$ arising from the loop integrals. A possible solution is to start with a $\overline{\text{DR}}$ renormalisation, and then reparametrise the quantities in the calculation without $\mathcal{O}(\epsilon^1)$ pieces. This, however, would not be convenient for a calculation initially based on the OS scheme.

While employing an $\overline{\text{MDR}}$ scheme for X_t allows avoiding the first issue of unphysical non-decoupling effects, the problem of mixed schemes persists. Thus, while at present it seems difficult to define a “best” scheme for X_t that would be suitable also for future higher-order evaluations, a mixed scheme where a $\overline{\text{MDR}}$ renormalisation of X_t is combined with an OS renormalisation of the stop masses appears to be the preferred choice in view of the currently available level of higher-order corrections.

6. Conclusions

An interesting possible feature of extensions of the SM with additional scalars is the existence of new types of interactions, like mass-dimensional trilinear couplings, which are not induced by a vacuum expectation value. In this article, we have focused on the

case of the MSSM, in which such a trilinear coupling controls the interaction between the scalar top quarks and the Higgs bosons, in the form of the stop mixing parameter X_t . In the event of a discovery of a BSM scalar sector, measuring the interactions between the different states will be of paramount importance to properly characterise the underlying model. We have discussed several approaches to access X_t via experimental measurements.

As a starting point, we illustrated the fact that the knowledge of just the two stop masses is not sufficient to determine X_t since additional information or some assumptions about the stop soft SUSY-breaking masses would be required in this case. While the measurement of the stop mixing angle in combination with measurements of the two stop masses can in principle be used to determine X_t together with the two stop soft SUSY-breaking masses, a precise determination of the stop mixing parameter is only possible in this way if the mass scale of the two stops is close to the TeV scale. The sensitivity to X_t rapidly deteriorates as the SUSY breaking scale increases. It should be stressed that this finding is valid even for the case of a collider of sufficient energy that has the capability for precise measurements of the stop masses and the stop mixing angle. The reason for the loss of sensitivity for higher values of M_{SUSY} are contributions that scale like m_t/M_{SUSY} . Another option that we investigated was extracting X_t from the measurement of a decay process like $\tilde{t}_2 \rightarrow \tilde{t}_1 + h$, but this has the disadvantage that the decay width, or its branching ratio, can be significantly suppressed if the stops are approximately mass-degenerate or in scenarios allowing other decays of stop quarks (e.g. if light electroweakinos are present).

As a result of our investigations, we found that the observable offering the best prospects for accessing X_t appears to be the mass of the SM-like Higgs boson, M_h . The parameter X_t enters the prediction for M_h starting from the one-loop level. We showed that with the input of the stop masses and of $\tan\beta$, the value of X_t can be determined from the measured value of M_h to a high level of accuracy. A further remarkable feature of the prediction for the mass of the SM-like Higgs boson in this context is that it retains a sizeable dependence on X_t even for SUSY scales as high as 100 TeV. Moreover, moderate variations of the SUSY breaking parameters do not alter the prediction of M_h very significantly. Thus, even if the knowledge of the SUSY spectrum is only quite limited, this is not expected to spoil the determination of X_t from M_h .

Next, we compared different possible choices of renormalisation schemes for the stop sector. The simplest option is to renormalise all stop-sector quantities, i.e. the stop masses and the mixing parameter, in the $\overline{\text{DR}}$ scheme. In addition to its simplicity, this choice can also be useful when investigating scenarios with high-scale boundary conditions employing the renormalisation-scale running of parameters. However, the $\overline{\text{DR}}$ scheme can also give rise to the known issue of unphysical non-decoupling effects — which for instance occur if there is a large hierarchy between the gluino and stop masses. One way to avoid such effects is to adopt an on-shell renormalisation scheme. While for the stop masses an OS renormalisation implies a unique definition of the counterterm, for X_t several choices are possible, depending on whether one relates the X_t counterterm to the calculation of a physical process, like e.g. $\tilde{t}_2 \rightarrow \tilde{t}_1 + h$, or whether one instead relates this counterterm to the counterterms of the stop mass matrix. Another choice

of renormalisation scheme that allows avoiding unphysical enhancements is the $\overline{\text{MDR}}$ scheme, in which the finite parts of the stop-mass and X_t counterterms are defined in such a way as to absorb the contributions involving powers of the gluino mass. We furthermore considered the possibility of adopting a mixed renormalisation scheme, i.e. renormalising some parameters on-shell but keeping others in the $\overline{\text{DR}}$ scheme. Such a choice, however, gives rise to the potential issue of a non-cancellation of ϵ^1 parts of loop integrals (from the three-loop level onwards), which changes the physical meaning of $\overline{\text{DR}}$ parameters compared to a pure $\overline{\text{DR}}$ scheme and prevents direct scheme conversions.

In the last part of our work, we considered the renormalisation of X_t in the specific context of the prediction for the mass of the SM-like Higgs boson. As we have demonstrated above that M_h is the most promising observable to determine X_t , it is crucial to assess to which extent the choices of the renormalisation prescription for X_t are compatible with the different approaches for computing M_h – fixed order, EFT, and hybrid. In a fixed-order calculation of M_h , adopting an OS renormalisation for X_t is a simple choice, which is straightforward to implement. On the other hand, when performing an EFT calculation of the Higgs mass, it is preferable to renormalise X_t in the $\overline{\text{DR}}$ or $\overline{\text{MDR}}$ scheme. This is also the case for hybrid computations, for which it is best to use a $\overline{\text{DR}}/\overline{\text{MDR}}$ scheme for the EFT part. This raises the issue of the conversion between OS and $\overline{\text{DR}}/\overline{\text{MDR}}$ schemes for X_t . We have pointed out the existence of possible large logarithmic terms in this conversion in the limit $M_{\text{SUSY}} \gg v$, which can cause a loss of accuracy of the entire M_h calculation. We have clarified the source of different types of large logarithmic terms and investigated the possibility of resumming them. A first type of large logarithms stems from the contribution involving the OS-scheme counterterm for the top-quark mass evaluated at $Q = M_{\text{SUSY}}$. These logarithms can be resummed via renormalisation-group running. However, a second, more problematic, type of terms arises from the finite part of the counterterm of the off-diagonal stop mass matrix when expanded in the $M_{\text{SUSY}} \gg v$ limit. These terms cannot be resummed with renormalisation group methods (a resummation within the framework of a soft-collinear effective theory should on the other hand in principle work), and moreover, their form depends on whether one performs the expansion in powers of v/M_{SUSY} for the case of degenerate or non-degenerate soft stop masses. We found that there exists no smooth transition between these two cases. Avoiding the expansion in v/M_{SUSY} is also not a viable option as this would mix orders of the EFT expansion in the M_h calculation. We, therefore, conclude that for the determination of the stop mixing parameter X_t from confronting a hybrid calculation of M_h with the measured value, the most advantageous choice is to adopt a $\overline{\text{DR}}/\overline{\text{MDR}}$ renormalisation for X_t . We note, however, that starting at the three-loop level this scheme will be affected by the problem related to uncanceled ϵ^1 parts of loop integrals described above.

Finally, we want to remark again that mass-dimensional trilinear couplings do not only appear in the MSSM but also in other BSM models. While the present study is focused on the stop mixing parameter in the MSSM, we expect that many of the difficulties identified in this study related to measuring and renormalising trilinear couplings will also appear in other models. Therefore, the situation can be expected to be more problematic in non-supersymmetric models, where the Higgs mass cannot be used to

constrain trilinear couplings. As we have shown, this is the case even if the new particles can be produced at the LHC or a future collider, and the corresponding mixing angle can be measured.

Acknowledgements

We thank Ivan Sobolev for collaboration in the early stages of this work, as well as Pietro Slavich for interesting discussions and helpful comments on our manuscript. J.B. and G.W. acknowledge support by the Deutsche Forschungsgemeinschaft (DFG, German Research Foundation) under Germany's Excellence Strategy – EXC 2121 “Quantum Universe” – 390833306. H.B. acknowledges support by the Alexander von Humboldt foundation. This work has been partially funded by the Deutsche Forschungsgemeinschaft (DFG, German Research Foundation) - 491245950.

A. Bottom-Yukawa corrections to the X_t conversion

In this Appendix, we present expressions for the conversion of X_t between the OS and the $\overline{\text{DR}}$ scheme including corrections controlled by the bottom Yukawa coupling.

In the case of $m_{\tilde{t}_L} = m_{\tilde{t}_R} = m_{\tilde{b}_L} = m_{\tilde{b}_R} = M_{\text{SUSY}}$, the finite part of the $\delta^{(1)}(m_t X_t)$ counterterm reads

$$\begin{aligned}
\delta^{(1)}(m_t X_t)|_{\text{fin}} &= \frac{\alpha_t}{4\pi} m_t X_t |\hat{X}_t|^2 \ln \frac{M_{\text{SUSY}}^2}{2m_t |X_t|} \\
&\quad + \frac{e^{i\phi_{X_t}} M_{\text{SUSY}}}{64\pi^2 v^2} \left(m_t |\hat{X}_t| - m_b |\hat{X}_b| \right)^3 \ln \frac{M_{\text{SUSY}}^2}{|m_t |X_t| - m_b |X_b|} \\
&\quad + \frac{e^{i\phi_{X_t}} M_{\text{SUSY}}}{64\pi^2 v^2} \left(m_t |\hat{X}_t| + m_b |\hat{X}_b| \right)^3 \ln \frac{M_{\text{SUSY}}^2}{|m_t |X_t| + m_b |X_b|} \\
&\quad + \text{non-log} = \\
&= \frac{3\alpha_t}{16\pi} m_t X_t |\hat{X}_t|^2 \ln \frac{M_{\text{SUSY}}^2}{M_t^2} + \frac{3\alpha_b}{16\pi} m_t X_t |\hat{X}_b|^2 \ln \frac{M_{\text{SUSY}}^2}{M_t^2} \\
&\quad + \text{non-log}, \tag{36}
\end{aligned}$$

in the limit $v/M_{\text{SUSY}} \rightarrow 0$. $\alpha_b \equiv y_b^2/(4\pi)$ with y_b being the bottom-Yukawa coupling.

For $m_{\tilde{t}_L} \neq m_{\tilde{t}_R}, m_{\tilde{b}_L} \neq m_{\tilde{b}_R}, m_{\tilde{t}_L} \neq m_{\tilde{b}_R}$, we obtain

$$\begin{aligned}
& \delta^{(1)}(m_t X_t) \Big|_{\text{fin}} = \\
& = \frac{\alpha_t}{8\pi} m_t X_t |\widehat{X}_t|^2 \left(\frac{2m_{\tilde{t}_L}}{m_{\tilde{t}_R}} \ln \frac{m_{\tilde{t}_L}^2}{|m_{\tilde{t}_L}^2 - m_{\tilde{t}_R}^2|} + \frac{m_{\tilde{t}_R}}{m_{\tilde{t}_L}} \ln \frac{m_{\tilde{t}_R}^2}{|m_{\tilde{t}_L}^2 - m_{\tilde{t}_R}^2|} \right) \\
& + \frac{\alpha_b}{8\pi} m_t X_t |\widehat{X}_b|^2 \left(-\frac{m_{\tilde{b}_R}(m_{\tilde{t}_L}^2 - 2m_{\tilde{t}_L}^2 + m_{\tilde{t}_R}^2)}{m_{\tilde{t}_L}(m_{\tilde{t}_L}^2 - m_{\tilde{t}_R}^2)} \ln \frac{m_{\tilde{b}_R}^2}{|m_{\tilde{b}_R}^2 - m_{\tilde{t}_L}^2|} \right. \\
& \quad + \frac{m_{\tilde{b}_R} m_{\tilde{t}_L} (m_{\tilde{b}_R}^2 - m_{\tilde{t}_R}^2)^2}{(m_{\tilde{b}_R}^2 - m_{\tilde{t}_L}^2) m_{\tilde{t}_R}^2 (m_{\tilde{t}_L}^2 - m_{\tilde{t}_R}^2)} \ln \frac{m_{\tilde{b}_R}^2}{|m_{\tilde{b}_R}^2 - m_{\tilde{t}_R}^2|} \\
& \quad \left. - \frac{m_{\tilde{b}_R} m_{\tilde{t}_L} (m_{\tilde{t}_L}^2 - m_{\tilde{t}_R}^2)}{m_{\tilde{t}_R}^2 (m_{\tilde{b}_R}^2 - m_{\tilde{t}_L}^2)} \ln \frac{m_{\tilde{t}_L}^2}{|m_{\tilde{t}_L}^2 - m_{\tilde{t}_R}^2|} + \frac{2m_{\tilde{b}_R} m_{\tilde{t}_L}}{m_{\tilde{b}_R}^2 - m_{\tilde{t}_L}^2} \ln \frac{m_{\tilde{b}_R}^2}{m_{\tilde{t}_L}^2} \right) \\
& + \dots, \tag{37}
\end{aligned}$$

where $\widehat{X}_b = X_b / \sqrt{m_{\tilde{b}_L} m_{\tilde{b}_R}}$. The ellipsis denotes further non-logarithmic terms. This means that the expression does not contain any terms $\propto \ln M_{\text{SUSY}}^2 / m_t^2$.

For $m_{\tilde{b}_L} = m_{\tilde{b}_R}, m_{\tilde{t}_L} \neq m_{\tilde{t}_R}$, we obtain

$$\delta^{(1)}(m_t X_t) \Big|_{\text{fin}} = \frac{\alpha_b}{16\pi} m_t X_t \frac{|X_b|^2}{m_{\tilde{b}_L}^2} \ln \frac{M_{\text{SUSY}}^2}{M_t^2} + \text{non-log}, \tag{38}$$

where here the non-logarithmic terms include logarithms not including a light SM mass (e.g. $\ln m_{\tilde{t}_L}^2 / |m_{\tilde{t}_L}^2 - m_{\tilde{t}_R}^2|$).

For $m_{\tilde{t}_L} = m_{\tilde{t}_R}, m_{\tilde{b}_L} \neq m_{\tilde{b}_R}$, the large logarithms in the conversion formula take the following form,

$$\delta^{(1)}(m_t X_t) \Big|_{\text{fin}} \supset \frac{3\alpha_t}{16\pi} m_t X_t \frac{|X_t|^2}{m_{\tilde{t}_L}^2} \ln \frac{M_{\text{SUSY}}^2}{M_t^2} + \text{non-log}. \tag{39}$$

To summarise, the conversion formula for the stop mixing parameter X_t in the heavy SUSY limit for the case of the scenarios with fully degenerate squark soft-breaking masses reads,

$$\begin{aligned}
X_t^{\overline{\text{DR}}}(M_{\text{SUSY}}) = X_t^{\text{OS}} \left\{ 1 + \left[\frac{\alpha_s}{\pi} - \frac{3\alpha_t}{16\pi} \left(1 - \frac{|X_t|^2}{M_{\text{SUSY}}^2} \right) \right. \right. \\
\left. \left. + \frac{3\alpha_b}{16\pi} \left(1 + \frac{|X_b|^2}{M_{\text{SUSY}}^2} \right) \right] \ln \frac{M_{\text{SUSY}}^2}{M_t^2} \right\} + \text{non-log}. \tag{40}
\end{aligned}$$

For the case where the stop soft-breaking masses are degenerate, but the sbottom soft-breaking masses are non-degenerate, this formula takes the form,

$$\begin{aligned}
X_t^{\overline{\text{DR}}}(M_{\text{SUSY}}) = X_t^{\text{OS}} \left\{ 1 + \left[\frac{\alpha_s}{\pi} - \frac{3\alpha_t}{16\pi} \left(1 - \frac{|X_t|^2}{m_{\tilde{t}_L}^2} \right) + \frac{3\alpha_b}{16\pi} \right] \ln \frac{M_{\text{SUSY}}^2}{M_t^2} \right\} \\
+ \text{non-log}. \tag{41}
\end{aligned}$$

If instead the sbottom soft-breaking masses are equal to each other but the stop soft-breaking masses are non-degenerate, the logarithmic terms in the conversion formula read,

$$X_t^{\overline{\text{DR}}}(M_{\text{SUSY}}) = X_t^{\text{OS}} \left\{ 1 + \left[\frac{\alpha_s}{\pi} - \frac{3\alpha_t}{16\pi} + \frac{3\alpha_b}{16\pi} \left(1 + \frac{|X_b|^2}{3m_{\tilde{b}_R}^2} \right) \right] \ln \frac{M_{\text{SUSY}}^2}{M_t^2} \right\} + \text{non-log.} \quad (42)$$

In all other cases the conversion formula reads,

$$X_t^{\overline{\text{DR}}}(M_{\text{SUSY}}) = X_t^{\text{OS}} \left\{ 1 + \left[\frac{\alpha_s}{\pi} - \frac{3\alpha_t}{16\pi} + \frac{3\alpha_b}{16\pi} \right] \ln \frac{M_{\text{SUSY}}^2}{M_t^2} \right\} + \text{non-log.} \quad (43)$$

References

- [1] ATLAS, “Observation of a new particle in the search for the Standard Model Higgs boson with the ATLAS detector at the LHC”, *Phys. Lett. B* **716** (2012) 1, 1207.7214.
- [2] CMS, “Observation of a New Boson at a Mass of 125 GeV with the CMS Experiment at the LHC”, *Phys. Lett. B* **716** (2012) 30, 1207.7235.
- [3] C.-Y. Chen, S. Dawson, and I. M. Lewis, “Exploring resonant di-Higgs boson production in the Higgs singlet model”, *Phys. Rev. D* **91** (2015) 035015, 1410.5488.
- [4] S. Kanemura, M. Kikuchi, and K. Yagyu, “Radiative corrections to the Higgs boson couplings in the model with an additional real singlet scalar field”, *Nucl. Phys. B* **907** (2016) 286, 1511.06211.
- [5] H. Bahl, J. Braathen, and G. Weiglein, “External leg corrections as an origin of large logarithms”, *JHEP* **02** (2022) 159, 2112.11419.
- [6] A. Bartl et al., “Search of stop, sbottom, tau sneutrino, and stau at an e^+e^- linear collider with $S^{**}(1/2) = 0.5\text{-TeV} - 2\text{-TeV}$ ”, *Z. Phys. C* **76** (1997) 549, [hep-ph/9701336](#).
- [7] M. Berggren et al., “Study of scalar top quarks at a future e^+e^- linear collider”, in: *4th International Workshop on Linear Colliders (LCWS 99)*, 1999 347, [hep-ph/9911345](#).
- [8] A. Bartl et al., “Phenomenology of stops, sbottoms, tau sneutrinos, and staus at an e^+e^- linear collider”, *Eur. Phys. J. direct* **2** (2000) 6, ed. by T. Behnke et al., [hep-ph/0002115](#).
- [9] A. Finch, H. Kluge, and A. Sopczak, “Precision measurements in the scalar top sector of the MSSM at a linear e^+e^- collider”, in: *International Workshop on Linear Colliders (LCWS 2002)*, 2002 259, [hep-ph/0211140](#).
- [10] K. Rolbiecki, J. Tattersall, and G. Moortgat-Pick, “Towards Measuring the Stop Mixing Angle at the LHC”, *Eur. Phys. J. C* **71** (2011) 1517, 0909.3196.
- [11] K. Desch et al., “LHC / LC interplay in the MSSM Higgs sector”, *JHEP* **09** (2004) 062, ed. by H. Videau and J. C. Brient, [hep-ph/0406322](#).
- [12] LHC/LC Study Group, “Physics interplay of the LHC and the ILC”, *Phys. Rept.* **426** (2006) 47, [hep-ph/0410364](#).
- [13] A. Djouadi, “Implications of the Higgs discovery for the MSSM”, *Eur. Phys. J. C* **74** (2014) 2704, 1311.0720.
- [14] R. El-Kosseifi et al., “The Higgs boson mass as fundamental parameter of the minimal supersymmetric standard model”, *Eur. Phys. J. C* **82** (2022) 657, 2202.06919.
- [15] H. Eberl, A. Bartl, and W. Majerotto, “SUSY QCD corrections to scalar quark pair production in e^+e^- annihilation”, *Nucl. Phys. B* **472** (1996) 481, [hep-ph/9603206](#).

- [16] A. Djouadi, W. Hollik, and C. Junger, “QCD corrections to scalar quark decays”, *Phys. Rev. D* **55** (1997) 6975, [hep-ph/9609419](#).
- [17] W. Beenakker et al., “Stop decays in SUSY QCD”, *Z. Phys. C* **75** (1997) 349, [hep-ph/9610313](#).
- [18] A. Djouadi et al., “Leading QCD corrections to scalar quark contributions to electroweak precision observables”, *Phys. Rev. D* **57** (1998) 4179, [hep-ph/9710438](#).
- [19] A. Bartl et al., “SUSY QCD corrections to stop and sbottom decays into W^{+-} and $Z0$ bosons”, *Phys. Lett. B* **419** (1998) 243, [hep-ph/9710286](#).
- [20] A. Bartl et al., “SUSY - QCD corrections to top and bottom squark decays into Higgs bosons”, *Phys. Rev. D* **59** (1999) 115007, [hep-ph/9806299](#).
- [21] J. Guasch, J. Sola, and W. Hollik, “Yukawa coupling corrections to scalar quark decays”, *Phys. Lett. B* **437** (1998) 88, [hep-ph/9802329](#).
- [22] S. Kraml, “Stop and sbottom phenomenology in the MSSM”, Master thesis, 1999, [hep-ph/9903257](#).
- [23] A. Brignole et al., “On the $O(\alpha(t)^2)$ two loop corrections to the neutral Higgs boson masses in the MSSM”, *Nucl. Phys.* **B631** (2002) 195, [hep-ph/0112177](#).
- [24] W. Hollik and H. Rzehak, “The Sfermion mass spectrum of the MSSM at the one loop level”, *Eur. Phys. J. C* **32** (2003) 127, [hep-ph/0305328](#).
- [25] S. Heinemeyer et al., “The Higgs sector of the complex MSSM at two-loop order: QCD contributions”, *Phys. Lett.* **B652** (2007) 300, [0705.0746](#).
- [26] N. Baro and F. Boudjema, “Automatised full one-loop renormalisation of the MSSM II: The chargino-neutralino sector, the sfermion sector and some applications”, *Phys. Rev. D* **80** (2009) 076010, [0906.1665](#).
- [27] T. Fritzsche et al., “Heavy Scalar Top Quark Decays in the Complex MSSM: A Full One-Loop Analysis”, *Phys. Rev. D* **86** (2012) 035014, [1111.7289](#).
- [28] T. Fritzsche et al., “The Implementation of the Renormalized Complex MSSM in FeynArts and FormCalc”, *Comput. Phys. Commun.* **185** (2014) 1529, [1309.1692](#).
- [29] W. Hollik and S. Paßehr, “Two-loop top-Yukawa-coupling corrections to the Higgs boson masses in the complex MSSM”, *Phys. Lett.* **B733** (2014) 144, [1401.8275](#).
- [30] W. Hollik and S. Paßehr, “Higgs boson masses and mixings in the complex MSSM with two-loop top-Yukawa-coupling corrections”, *JHEP* **10** (2014) 171, [1409.1687](#).
- [31] S. Paßehr, “Two-Loop Corrections to the Higgs-Boson Masses in the Minimal Supersymmetric Standard Model with CP-Violation”, PhD thesis, München, Tech. U., 2014, <http://mediatum.ub.tum.de?id=1223795> ().
- [32] M. Frank et al., “The Higgs Boson Masses and Mixings of the Complex MSSM in the Feynman-Diagrammatic Approach”, *JHEP* **02** (2007) 047, [hep-ph/0611326](#).
- [33] A. Djouadi, J. Kalinowski, and M. Spira, “HDECAY: A Program for Higgs boson decays in the standard model and its supersymmetric extension”, *Comput. Phys. Commun.* **108** (1998) 56, [hep-ph/9704448](#).

- [34] A. Djouadi, J.-L. Kneur, and G. Moultaka, “SuSpect: A Fortran code for the supersymmetric and Higgs particle spectrum in the MSSM”, *Comput. Phys. Commun.* **176** (2007) 426, [hep-ph/0211331](#).
- [35] M. Muhlleitner, A. Djouadi, and Y. Mambrini, “SDECAY: A Fortran code for the decays of the supersymmetric particles in the MSSM”, *Comput. Phys. Commun.* **168** (2005) 46, [hep-ph/0311167](#).
- [36] A. Djouadi, M. M. Muhlleitner, and M. Spira, “Decays of supersymmetric particles: The Program SUSY-HIT (SUSpect-SdecaY-Hdecay-InTerface)”, *Acta Phys. Polon. B* **38** (2007) 635, ed. by K. Fialkowski and B. Muryn, [hep-ph/0609292](#).
- [37] P. Slavich et al., “Higgs-mass predictions in the MSSM and beyond”, *Eur. Phys. J. C* **81** (2021) 450, ed. by P. Slavich and S. Heinemeyer, [2012.15629](#).
- [38] E. Bagnaschi et al., “MSSM Higgs Boson Searches at the LHC: Benchmark Scenarios for Run 2 and Beyond”, *Eur. Phys. J. C* **79** (2019) 617, [1808.07542](#).
- [39] H. Bahl, S. Liebler, and T. Stefaniak, “MSSM Higgs benchmark scenarios for Run 2 and beyond: the low $\tan \beta$ region”, *Eur. Phys. J. C* **79** (2019) 279, [1901.05933](#).
- [40] ATLAS, “Interpretations of the combined measurement of Higgs boson production and decay”, (2020), [ATLAS-CONF-2020-053](#).
- [41] S. Heinemeyer, W. Hollik, and G. Weiglein, “FeynHiggs: A Program for the calculation of the masses of the neutral CP even Higgs bosons in the MSSM”, *Comput. Phys. Commun.* **124** (2000) 76, [hep-ph/9812320](#).
- [42] S. Heinemeyer, W. Hollik, and G. Weiglein, “The Masses of the neutral CP - even Higgs bosons in the MSSM: Accurate analysis at the two loop level”, *Eur. Phys. J. C* **9** (1999) 343, [hep-ph/9812472](#).
- [43] T. Hahn et al., “FeynHiggs: A program for the calculation of MSSM Higgs-boson observables - Version 2.6.5”, *Comput. Phys. Commun.* **180** (2009) 1426.
- [44] G. Degrand et al., “Towards high precision predictions for the MSSM Higgs sector”, *Eur. Phys. J. C* **28** (2003) 133, [hep-ph/0212020](#).
- [45] T. Hahn et al., “High-Precision Predictions for the Light CP -Even Higgs Boson Mass of the Minimal Supersymmetric Standard Model”, *Phys. Rev. Lett.* **112** (2014) 141801, [1312.4937](#).
- [46] H. Bahl and W. Hollik, “Precise prediction for the light MSSM Higgs boson mass combining effective field theory and fixed-order calculations”, *Eur. Phys. J. C* **76** (2016) 499, [1608.01880](#).
- [47] H. Bahl et al., “Reconciling EFT and hybrid calculations of the light MSSM Higgs-boson mass”, *Eur. Phys. J. C* **78** (2018) 57, [1706.00346](#).
- [48] H. Bahl et al., “Precision calculations in the MSSM Higgs-boson sector with FeynHiggs 2.14”, *Comput. Phys. Commun.* **249** (2020) 107099, [1811.09073](#).
- [49] P. Bechtle et al., “The Light and Heavy Higgs Interpretation of the MSSM”, *Eur. Phys. J. C* **77** (2017) 67, [1608.00638](#).

- [50] W. G. Hollik, G. Weiglein, and J. Wittbrodt, “Impact of Vacuum Stability Constraints on the Phenomenology of Supersymmetric Models”, JHEP **03** (2019) 109, 1812.04644.
- [51] H. Bahl et al., “Theoretical uncertainties in the MSSM Higgs boson mass calculation”, Eur. Phys. J. C **80** (2020) 497, 1912.04199.
- [52] Y. Yamada, “Gauge dependence of the on-shell renormalized mixing matrices”, Phys. Rev. **D64** (2001) 036008, hep-ph/0103046.
- [53] G. Degrassi, P. Slavich, and F. Zwirner, “On the neutral Higgs boson masses in the MSSM for arbitrary stop mixing”, Nucl. Phys. B **611** (2001) 403, hep-ph/0105096.
- [54] S. Heinemeyer et al., “High-precision predictions for the MSSM Higgs sector at $O(\alpha(b)\alpha(s))$ ”, Eur. Phys. J. **C39** (2005) 465, hep-ph/0411114.
- [55] A. Dedes, G. Degrassi, and P. Slavich, “On the two loop Yukawa corrections to the MSSM Higgs boson masses at large $\tan\beta$ ”, Nucl. Phys. **B672** (2003) 144, hep-ph/0305127.
- [56] M. Muhlleitner, H. Rzehak, and M. Spira, “MSSM Higgs Boson Production via Gluon Fusion: The Large Gluino Mass Limit”, JHEP **04** (2009) 023, 0812.3815.
- [57] P. Kant et al., “Light MSSM Higgs boson mass to three-loop accuracy”, JHEP **08** (2010) 104, 1005.5709.
- [58] J. Braathen, M. D. Goodsell, and P. Slavich, “Leading two-loop corrections to the Higgs boson masses in SUSY models with Dirac gauginos”, JHEP **09** (2016) 045, 1606.09213.
- [59] J. Aebischer et al., “The MSSM without Gluinos; an Effective Field Theory for the Stop Sector”, Eur. Phys. J. C **77** (2017) 740, 1703.08061.
- [60] M. Krämer, B. Summ, and A. Voigt, “Completing the scalar and fermionic Universal One-Loop Effective Action”, JHEP **01** (2020) 079, 1908.04798.
- [61] T. Deppisch and U. Nierste, “Little hierarchies solve the little fine-tuning problem: a case study in supersymmetry with heavy gluinos”, (2019), 1908.01222.
- [62] H. Bahl, I. Sobolev, and G. Weiglein, “Precise prediction for the mass of the light MSSM Higgs boson for the case of a heavy gluino”, Phys. Lett. B **808** (2020) 135644, 1912.10002.
- [63] S. Borowka et al., “Renormalization scheme dependence of the two-loop QCD corrections to the neutral Higgs-boson masses in the MSSM”, Eur. Phys. J. C **75** (2015) 424, 1505.03133.
- [64] D. Meuser, PhD thesis, Hamburg U., *in preparation*.
- [65] G. Degrassi, S. Di Vita, and P. Slavich, “Two-loop QCD corrections to the MSSM Higgs masses beyond the effective-potential approximation”, Eur. Phys. J. C **75** (2015) 61, 1410.3432.

- [66] E. Bagnaschi, J. Pardo Vega, and P. Slavich, “Improved determination of the Higgs mass in the MSSM with heavy superpartners”, *Eur. Phys. J. C* **77** (2017) 334, 1703.08166.